A fully well-balanced scheme for the 1D blood flow equations with friction source term

Beatrice Ghitti[1,*], Christophe Berthon[2], Minh Hoang LE[3], Eleuterio F. Toro[4]

Abstract

We consider the 1D blood flow equations with friction source term. The main purpose of this work is the derivation of a positivity preserving and fully well-balanced scheme, which correctly approximates the solutions of this system, exactly preserves all the associated steady states, including the moving ones, and ensures the positivity of the cross-sectional area. To address such issues, a study of the moving steady states related to the friction source term is first performed. Afterwards, a Godunov-type scheme is constructed, by deriving a two-state approximate Riemann solver and by introducing a relevant discretization of the source term, to enforce the well-balanced property. The scheme is then adapted to the generalized model including a space-variable viscous resistance; a second-order well-balanced MUSCL extension of the scheme is also proposed. Numerical experiments are finally carried out in order to validate the scheme and highlight its properties.

Keywords: 1D blood flow, friction source term, moving steady states, Godunov-type scheme, fully well-balanced scheme, positivity preserving scheme.

1. Introduction

The goal of this paper is to derive a numerical scheme to approximate the weak solutions of the one-dimensional blood flow equations in arteries with friction source term. In fact, one-dimensional blood flow models are nowadays widely used in the field of cardiovascular mathematics and biomedical engineering, with an extremely vast range of relevant applications. These models can be used as stand-alone tools, in the description of flow patterns, pressure wave propagation and average velocities in a single vessel or in networks of vessels [1, 9, 22, 6, 19]. On the other hand, combined together with lumped-parameter (or zero-dimensional) models, one-dimensional models play a crucial role in the attempt to construct global, closed-loop, multi-scale mathematical models of the human circulation system, including several intercommunicating components, namely the arterial system, the venous system, the heart, the pulmonary circulation and the microcirculation [20]. Hence, the numerical discretization of the governing equations of these models and the development of accurate and efficient numerical schemes able

[*]Corresponding author.
Email address: `beatrice.ghitti@unitn.it` (Beatrice Ghitti)
[1]Department of Mathematics, University of Trento, Trento, Italy
[2]Laboratoire de Mathématiques Jean Leray, University of Nantes, Nantes, France
[3]Laboratoire d'Hydraulique Saint-Venant (ENPC, EDF R&D, CEREMA), Chatou, France
[4]Laboratory of Applied Mathematics DICAM, University of Trento, Italy

to correctly approximate their solutions represent urgent challenges to be constantly addressed.
From a numerical point of view, the source term discretization needs a particular focus, since it may involve large errors in the simulations. In order to get correct approximation of the source terms, the well-balanced strategy leads to more accurate numerical methods. The idea is that, in the absence of time derivatives, the schemes must respect the correct balance between the advective term, namely the flux, and the source term. Moreover, as remarked by the authors in [18], the well-balanced property is not only a desirable feature of numerical schemes for exactly solving steady problems, but this is also an important property to correctly compute solutions to time-dependent problems with source terms, specially of the geometric type.
Then, the main focus of this paper stands in the derivation of relevant discretizations of the flux and the source term of the system under study, so as to produce a fully well-balanced numerical scheme which exactly preserve all the steady state solutions, both at rest and moving steady states, of the one-dimensional blood flow model.

The numerical preservation of steady states has been of prime importance during the last two decades, especially for the shallow-water equations. Originally, the *well-balanced property* of a scheme was introduced as the ability of a scheme to exactly preserve the steady states at rest, or non-moving steady states, namely the steady state solutions with vanishing velocity. For the shallow-water equations, these particular solutions are the so-called *lake at rest* steady states. This work was pioneered by Bermudez and Vazquez [3], as well as by Greenberg and LeRoux [13]. In [3], the authors introduced the condition called *conservation property* or *C-property*: a scheme is said to satisfy this condition if it solves correctly the steady states at rest of the shallow-water equations. The term of well-balanced scheme was then coined by Greenberg and LeRoux in [13], where they defined a well-balanced scheme as a numerical scheme able to exactly preserve solutions at rest. Later, this definition was extended to yield the *fully well-balanced property*, as the ability of a scheme to preserve all the steady states, including the moving ones, where the velocity does not vanish. Gosse [12] first extended this approach to construct a well-balanced scheme for the shallow-water equations able to preserve all the steady states, both non-moving and moving steady states, with the additional requirement of approximately solving the governing non-linear Bernoulli's equation. This work was then simplified by Audusse *et al.* [2], who focused again on the steady states at rest of the shallow-water equations and proposed the well-known hydrostatic reconstruction technique, which ensures the preservation of non-moving steady states, without needing to solve a non-linear equation. This technique allows to obtain a well-balanced numerical scheme by means of a local modification, the so-called hydrostatic reconstruction, of states, in such a way that stationary solutions corresponding to water at rest situations are preserved. However, the derivation of the hydrostatic reconstruction technique in [2] was strongly related to the particular nature of the shallow-water system and to the easy expression of the water at rest solutions. Then, Castro *et al.* [7] proposed a more abstract and general derivation of the hydrostatic reconstruction for the shallow-water system, so that it can be extended to more general stationary solutions and hyperbolic systems with source terms.
Most of the above cited references deal only with the lake at rest steady states and they do not consider the steady states in their full generality. In the literature, a few attempts to design a numerical strategy able to restore all the steady states can be found. In this regard, we cite again [7], for example, where the main idea stays in a suitable

extension of the hydrostatic reconstruction. The resulting scheme is able to restore all the steady states, but the scheme fails preserving the positiveness of the water height. Later on, in [4, 5] an extension of the work by Gosse [12] was designed in order to deal with Godunov-type schemes. In particular, in [4] the authors suggested a numerical scheme that is fully well-balanced, i.e. it captures all the moving and non-moving steady states, robust, i.e. it preserves the positivity of the water height, and entropy-satisfying, namely it satisfies a discrete entropy inequality. Thereafter, Berthon *et al.* [5] proposed an easy to implement Godunov-type scheme which is positive, fully well-balanced and based on the derivation of a simple approximate Riemann solver. Interestingly, this solver was derived from a suitable linearization of the numerical method described in [4]. Finally, we mention the more recent works [16, 17], where the authors derived a non-negativity preserving and well-balanced numerical scheme for the shallow-water equations with topography and/or Manning friction, which preserves the associated steady states, including the moving ones. The Godunov-type scheme was obtained by using a relevant average of the source terms within the scheme, in order to enforce the required well-balanced property.

The issue of well-balanced schemes also for one-dimensional blood flow has already been addressed in the past, even if less work has been done so far with respect to the shallow-water equations. For example, in the framework of the hydrostatic reconstruction [2], Delestre and Lagrée [8] proposed a well-balanced finite-volume scheme able to exactly preserve the steady states at rest, in the case of a single variable parameter, namely variable reference cross-sectional area. Müller *et al.* [18] used the simplified mathematical model introduced by Toro and Siviglia [25] as a starting point to construct a well-balanced, high-order, path-conservative numerical scheme for one-dimensional blood flow in elastic vessels with varying mechanical properties. The proposed numerical scheme in [18] was constructed following the generalized hydrostatic reconstruction technique [7], based on a particular choice of family of integration paths within the framework of path-conservative methods, introduced by Parés [21], which guarantees exact well-balanced properties for any steady solution. Thereafter, Müller and Toro [19] presented an extension of this scheme to models that include the variation of other parameters, such as the cross-sectional area at a reference state and the external pressure. Starting from the more realistic mathematical model proposed by Toro and Siviglia [26], in [19] the authors extended the well-balanced, high-order numerical scheme for solving the 1D blood flow model in vessels with variable geometrical and mechanical properties, still within the framework of path-conservative finite-volume type schemes.
In all the above cited works, one or more variable vessel properties were considered and additional source terms arose from the variation of these geometrical or mechanical properties, the so-called *geometric-type* source terms. By means of the well-balanced strategy, these geometric-type source terms were suitably treated and discretized, in a way that the resulting well-balanced numerical schemes were able to correctly compute both steady and unsteady solutions. However, the authors limited themselves to develop well-balanced schemes that only preserve steady states at rest, where the velocity u vanishes. Therefore, since the techniques proposed and adopted so far allow the preservation of some steady states, namely the non-moving ones, but they fail whenever moving steady states are involved, in this paper we tackle the necessity to establish a completely new strategy in order to derive fully well-balanced schemes. Then, the main objective of the present work is to design a new numerical approach to build a fully well-balanced scheme for the one-dimensional blood flow model, for both non-moving and

moving steady states. In particular, the derivation of such a scheme, in the framework of Godunov-type schemes, is based on a suitable definition of the approximate Riemann solver and a relevant discretization of the friction source term within the Riemann solver, so as to ensure the well-balanced property of the complete numerical scheme. This innovative procedure is a modification/extension of the technique constructed for the shallow-water equations with topography and/or Manning friction in [16, 17]. Actually, we will appreciate in the next sections that the strategy here proposed for the blood flow equations with friction source term contains also some interesting novelties, such as, for instance, a generalization of the well-established blood flow model, which includes a viscous resistance R that is no longer a constant parameter, but a prescribed function with respect to the space variable x, i.e. $R \equiv R(x)$.
In addition to the well-balanced property, usually there are other nice properties for a scheme to possess. Therefore, the numerical scheme we are going to derive will satisfy the following properties:

- consistency;
- well-balancing, i.e. preservation of all the steady states, including the moving ones;
- robustness, i.e. preservation of the positivity of the cross-sectional area.

In this starting work, no geometric-type source terms are considered, but all geometrical and mechanical properties of the vessel are assumed to be uniform in space, along the vessel length, and the only source term included in the model is the friction source term. This work aims to be a first step towards a more general and efficient strategy for the numerical treatment of any source terms, the friction source term, as well as the geometric-type source terms arising from variable geometrical and mechanical properties, to construct fully well-balanced numerical schemes suited for the one-dimensional blood flow model.

The paper is organized as follows. In Section 2 we briefly present the governing equations of one-dimensional blood flow with friction source term under consideration and we study the steady state solutions of the system. Then, in Section 3 we propose a Godunov-type scheme that is fully well-balanced for our blood flow system. In this section, we first recall some generalities about Godunov-type schemes, then we derive the fully well-balanced scheme for the model with constant viscous resistance, by adopting the HLLC approach in the definition of the intermediate states of the approximate Riemann solver and by introducing a relevant discretization of the friction source term, so that the well-balanced property is ensured. We conclude this section by extending the derived fully well-balanced scheme to the generalized model with variable viscous resistance. Afterwards, in Section 4 we state and prove all the properties satisfied by the numerical scheme, in addition to the well-balanced property. Thereafter, in Section 5 the scheme is extended to be second-order accurate. In particular, since the well-balancing is lost by this extension, we show how to recover this essential feature. Finally, in Section 6 we present different sets of numerical experiments and discuss the obtained results, in order to validate the derived well-balanced scheme and assess its properties. We conclude with Section 7, where final remarks are made and perspectives for future work are outlined.

2. 1D blood flow model with friction source term

In this section we succinctly present the governing equations for the one-dimensional blood flow model under consideration. Thereafter, we focus on the study of the steady state solutions of this system, arising from the friction source term.

2.1. Mathematical model

The one-dimensional blood flow model under study results from averaging the full 3D time-dependent incompressible Navier-Stokes equations over the vessel cross section, assuming that the characteristic axial length-scale is much longer than the radial one and that the flow is axisymmetric. The structural mechanics of the vessel wall is also simplified, by assuming radial displacement and elastic material properties, since the elastic response is assumed to be the dominating effect in the vessel wall dynamics. Even under such strong simplifications of reality, this model preserves the essential physical features of wave propagations in compliant vessels, providing accurate predictions of pressure and flow waveforms in all main arteries. For a full derivation and description of the model the reader is referred to [10, 24], for instance.
A well-established non-conservative formulation for one-dimensional blood flow is given by the following system:

$$\begin{cases} \partial_t A + \partial_x q = 0, \\ \partial_t q + \partial_x \left(\widehat{\alpha} \dfrac{q^2}{A} \right) + \dfrac{A}{\rho} \partial_x p = f, \end{cases} \tag{1}$$

where $x \in \mathbb{R}$ is the axial coordinate along the vessel and $t > 0$ is time. The variables involved in this model are the cross-sectional area $A(x,t) > 0$ of the vessel and the flow rate $q(x,t) \in \mathbb{R}$. We also define the blood flow velocity $u(x,t)$ such that $q = Au$. The Coriolis coefficient $\widehat{\alpha}$ depends on the assumed velocity profile and, in our case, $\widehat{\alpha} \equiv 1$ is a quite realistic assumption, which describes a flat velocity profile; ρ is the constant blood density, $p(x,t) > 0$ is the average internal pressure and $f(x,t)$ is the friction force per unit length, modelled as follows:

$$f(x,t) = -R(x)u = -R(x)\frac{q}{A}, \tag{2}$$

where the viscous resistance $R(x) > 0$ is a prescribed function with respect to the space variable x. We emphasize that, in the well-known 1D model, R is taken as a constant parameter, given by:

$$R = \gamma \pi \upsilon, \tag{3}$$

where υ is the kinematic viscosity, defined as $\upsilon = \frac{\mu}{\rho}$, with μ being the dynamic viscosity. Moreover, in this work we fix $\gamma = 22$, as specified in [1].
To be closed, system (1) must be completed with a pressure law, which links the mean pressure p with the cross-sectional area A. In the present work, the purely elastic tube law is considered as closure condition to describe the elastic deformation of the arterial wall with variations of the transmural pressure, defined as follows:

$$p(x,t) = p_{ext}(x,t) + K(x) \left[\left(\frac{A(x,t)}{A_0(x)} \right)^m - \left(\frac{A(x,t)}{A_0(x)} \right)^n \right], \tag{4}$$

where $p_{ext}(x,t)$ is the external pressure acting on the vessel and the second term in (4) is the transmural pressure. The pressure p also depends parametrically on the

cross-sectional area at rest A_0 and on a set of coefficients embedded in the factor $K(x)$, which account for physical and mechanical characteristics of the vessel. The parameters m and n are obtained form higher order models or simply computed from experimental measurements. In general, $m > 0$ and $n \in (-2; 0]$. In this work, we consider the typical values for arteries, namely $m = \frac{1}{2}$ and $n = 0$.
The elastic tube law (4) comes from the mechanical model used to describe the vessel wall dynamics, based on the simplified assumption of an instantaneously elastic equilibrium, according to which the vessel wall responds to a change in the fluid pressure by adapting its section area, following a perfectly elastic law [9].
Point 1. This is an useful law that can be adopted in practice. Indeed, the elastic behaviour of vessel walls is considered to be the dominating effect, so that the viscous effects of vessel walls can be neglected in the 1D model, which, under this strong assumption, is still able to reproduce the main characteristic features of wave propagation phenomena in compliant vessels. End point 1.
The positive function $K(x)$ in (4) denotes the arterial stiffness and it is modelled as in [24, 10] by:

$$K(x) = \frac{\sqrt{\pi} h_0(x) E(x)}{(1 - \nu^2)\sqrt{A_0(x)}}, \tag{5}$$

where $A_0(x) = \pi r_0(x)^2$ is the vessel cross-sectional area at equilibrium, with $r_0(x)$ being the vessel radius at rest, $h_0(x)$ is the vessel wall-thickness, $E(x)$ is the Young's modulus and ν is the Poisson ratio. For incompressible vessel walls, we adopt the value $\nu = 0.5$.
In the present work, we assume that the geometrical and mechanical properties of the vessel are independent of x, i.e. A_0, h_0, E, K and p_{ext} are all taken as constant parameters. Point 1. Including non-constant vessel parameters, such as the arterial stiffness K, in the model would result in a more realistic 1D model, but coming at the cost that additional geometric-type source terms would arise, which should be suitably treated and discretized in order to preserve the properties of the scheme we have in mind. However, this is not the aim of this starting work. End point 1.
Under these assumptions, computing the pressure gradient in system (1) and setting:

$$\gamma = \frac{K}{3\rho\sqrt{A_0}} \; : \; constant, \tag{6}$$

we get the final form of the one-dimensional blood flow model with elastic tube law and friction source term, which reads:

$$\begin{cases} \partial_t A + \partial_x q = 0, \\ \partial_t q + \partial_x \left(\dfrac{q^2}{A} + \gamma A^{3/2} \right) = -Ru. \end{cases} \tag{7}$$

From now on, system (7) will be the main model under study, where the viscous resistance R will be taken either as a constant or as a prescribed function with respect to x.
In particular, system (7) including a variable viscous resistance $R(x)$ represents an interesting extension of the well-known simplified model with constant R. From a modelling point of view, selecting a correct and physically relevant function for $R(x)$ may allow to describe and model some real physiological or pathological cases of biomedical interest depending on a variable resistance R, or to simulate and analyse the effects on pressure and flow of this physical property of the system. For this reason, we are interested in considering such a generalization of the usual blood flow system. Moreover,

as we will discuss in Section 6, this generalized model will represent a very useful tool in the well-balanced assessment of the derived numerical scheme.
In order to shorten the notations, we can rewrite system (7) under the classical form of conservation laws with a source term:

$$\partial_t W + \partial_x F(W) = S(W),$$

where we have introduced the following definitions:

$$W = \begin{pmatrix} w_1 \\ w_2 \end{pmatrix} \equiv \begin{pmatrix} A \\ q \end{pmatrix}, \quad F(W) = \begin{pmatrix} q \\ \dfrac{q^2}{A} + \gamma A^{3/2} \end{pmatrix} \quad \text{and} \quad S(W) = \begin{pmatrix} 0 \\ -R\dfrac{q}{A} \end{pmatrix}. \tag{8}$$

In the present work, in order to not violate the physical meaning of the variable A, we assume that the cross-sectional area A never vanishes. Then, the conserved variables W lie in the following set of admissible states Ω, which prescribes a physically admissible positive cross-sectional area:

$$\Omega = \left\{ W = (A, q)^T \in \mathbb{R}^2 \,:\, A > 0,\, q \in \mathbb{R} \right\} \subset \mathbb{R}^2.$$

Namely, collapse of blood vessels is not admitted here.
For the sake of convenience, we introduce here also the wave speed, denoted by c, as follows:

$$c^2 = \frac{3}{2}\gamma\sqrt{A}. \tag{9}$$

2.2. Steady states with friction source term

Now, we propose to study the steady states of system (7). The steady state solutions of the blood flow equations are a specific class of solutions of system (7) for which the time derivatives vanish, namely:

$$W = (A, q)^T \in \Omega \quad \text{such that} \quad \partial_t W = 0.$$

One important issue to be addressed in this work lies in the investigation of such solutions. In particular, because of the presence of the source term, these solutions are non-trivial. To exhibit the steady states, we first consider the blood flow model (7) with constant viscous resistance R; afterwards, we turn to the case of variable parameter $R(x)$ and we extend the study of these solutions also to this more general framework.

First, let us assume $R > 0$ be a given constant, modelled as in (3). Then, by imposing the solution of (7) to be a steady state, we get the following system:

$$\begin{cases} \partial_x q = 0, \\ \partial_x \left(\dfrac{q^2}{A} + \gamma A^{3/2} \right) = -R\dfrac{q}{A}. \end{cases} \tag{10}$$

From the first equation in (10), we immediately obtain that the discharge q must be uniform in space. As a consequence, we denote this uniform flow rate as follows:

$$q = q_0 \,:\, \textit{constant}. \tag{11}$$

On the one hand, if $q_0 = 0$, then the blood velocity u also vanishes and the steady states (10) are said at rest or non-moving steady states; on the other hand, if $q_0 \neq 0$, we deal

with the so-called moving steady states. In the following, we are interested in studying the steady state solutions (10) of the blood flow model in their full generality, namely in the case where q_0 does not vanish.
Using q_0 within the second equation of (10) yields:

$$\partial_x \left(\frac{q_0^2}{A} + \gamma A^{3/2} \right) = -Rq_0 \frac{1}{A}, \tag{12}$$

where we assume the function A to be smooth, at least of class C^1. Then, the solution of the non-linear ordinary differential equation (12) is the cross-sectional area $A(x) > 0$ for a steady state with uniform discharge q_0. After straightforward computations, we rewrite (12) under the following form:

$$\partial_x \left(-q_0^2 \log A + \frac{3}{5}\gamma A^{5/2} \right) = -Rq_0. \tag{13}$$

Now, let us fix the value of the constant discharge $q_0 \neq 0$ and $x_0 \in \mathbb{R}$ as an arbitrary reference point, and introduce the initial condition $A(x_0) = A_{ref}$, that is the value of the cross-sectional area at the point x_0. For all $x \in \mathbb{R}$, we integrate equation (13) over the interval (x_0, x) to get:

$$-q_0^2 \log A + \frac{3}{5}\gamma A^{5/2} = -q_0^2 \log A_{ref} + \frac{3}{5}\gamma A_{ref}^{5/2} - Rq_0(x - x_0). \tag{14}$$

The above relation turns out to be a strongly non-linear equation, which characterizes the unknown $A := A(x)$. The solution of the non-linear equation (14) represents the steady state cross-sectional area A with uniform flow rate q_0.
In order to shorten the notations, we rewrite (14) in the following form:

$$\mathcal{F}_{q_0}(A) - \mathcal{F}_{q_0}(A_{ref}) + Rq_0(x - x_0) = 0, \tag{15}$$

where the following function has been introduced:

$$\mathcal{F}_{q_0}(A) = -q_0^2 \log A + \frac{3}{5}\gamma A^{5/2}. \tag{16}$$

In order to exhibit solutions of equation (15), we first study the function $\mathcal{F}_{q_0}(A)$. The derivative of $\mathcal{F}_{q_0}$ with respect to A is given by:

$$\frac{\partial \mathcal{F}_{q_0}}{\partial A}(A) = -\frac{q_0^2}{A} + \frac{3}{2}\gamma A^{3/2}.$$

Next, let us define the critical value A_c such that $\frac{\partial \mathcal{F}_{q_0}}{\partial A}(A_c) = 0$, as follows:

$$A_c = \left(\frac{2}{3} \frac{q_0^2}{\gamma} \right)^{2/5} > 0, \tag{17}$$

Then, we easily obtain that the function $A \mapsto \mathcal{F}_{q_0}(A)$ is strictly increasing on $(A_c, +\infty)$, while it is strictly decreasing on $(0, A_c)$. As a consequence, it admits a unique minimum point in $(0, +\infty)$ and this minimum is reached for $A = A_c$, as depicted in Figure 1.
Now, we have to solve:

$$\mathcal{F}_{q_0}(A) = \mathcal{F}_{q_0}(A_0) - Rq_0(x - x_0). \tag{18}$$

Since the right hand side of (18) is fixed, we set, for any $x \in \mathbb{R}$,

$$\alpha_0(x) = \mathcal{F}_{q_0}(A_{ref}) - Rq_0(x - x_0),$$

so that we can write $\mathcal{F}_{q_0}(A(x)) = \alpha_0(x)$, and then we have:

(i) if $\mathcal{F}_{min} = \mathcal{F}_{q_0}(A_c) > \alpha_0$, then equation (18) has no solution;

(ii) if $\mathcal{F}_{min} = \alpha_0$, then equation (18) admits exactly one unique solution, that is $A = A_c$;

(iii) if $\mathcal{F}_{min} < \alpha_0$, then equation (18) has two admissible steady state solutions.

These three possibilities are depicted in Figure 1, together with the function $\mathcal{F}_{q_0}(A)$. Equation (18) can not be solved explicitly, therefore an iterative procedure can be used. The resulting steady state solutions are displayed in Figure 1.

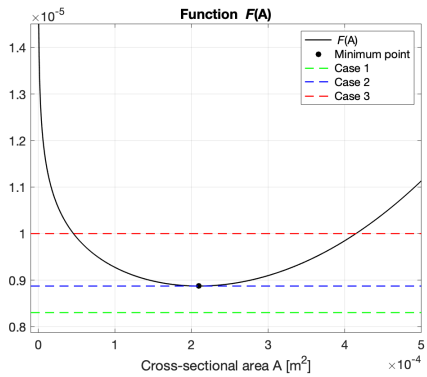

(a)

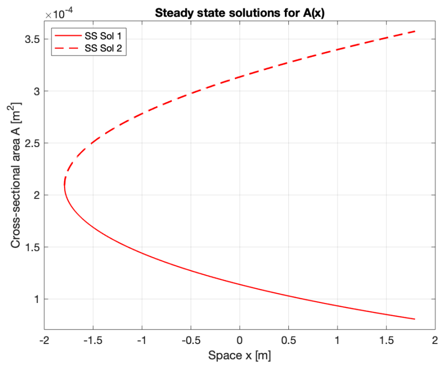

(b)

Figure 1: (a) Plot of the function $\mathcal{F}_{q_0}(A)$ given by (16) and of its minimum point A_c given by (17), for fixed uniform discharge $q_0 = -10^{-3}$ m^3/s. (b) Plot of the steady state solutions for the cross-sectional area $A(x)$, for $q_0 = -10^{-3}$ m^3/s, $x_0 = 0$ and $A_{ref} = A_0$, computed by using the Newton-Raphson method.

In conclusion, we have obtained the general form of the steady state solutions of the blood flow equations (7) with friction source term and constant viscous resistance R. We stress the fact that these steady states are parametrized by the choice of x_0 and A_{ref}.

Next, we turn to the generalized model, which includes a viscous resistance $R(x)$ given by a prescribed function with respect to the space variable x. The steady state solutions of the generalized model are now given by:

$$\begin{cases} q = q_0, \\ \mathcal{F}_{q_0}(A) - \mathcal{F}_{q_0}(A_{ref}) = -q_0 \displaystyle\int_{x_0}^{x} R(\xi)\, d\xi, \end{cases} \tag{19}$$

where the function $\mathcal{F}_{q_0}$ is defined by (16).
The integral of the function R in (19) is approximated by a quadrature formula to be chosen suitably and we denote it as follows:

$$\mathcal{Q}(R, x_0, x) \approx \int_{x_0}^{x} R(\xi)\, d\xi. \tag{20}$$

Assume that the value of the uniform discharge q_0, the reference point x_0 and the initial condition $A(x_0) = A_{ref}$ are given values. Then, the steady state for the cross-sectional area A at the point $x_i \in \mathbb{R}$, namely $A_i = A(x_i)$, is computed as:

$$
\begin{aligned}
\mathcal{F}_{q_0}(A_i) - \mathcal{F}_{q_0}(A_{ref}) &= \sum_{j=0}^{i-1} \Big(\mathcal{F}_{q_0}(A_{j+1}) - \mathcal{F}_{q_0}(A_j)\Big) \\
&= -q_0 \sum_{j=0}^{i-1} \int_{x_j}^{x_{j+1}} R(x)\,dx \\
&\approx -q_0 \sum_{j=0}^{i-1} \mathcal{Q}(R, x_j, x_{j+1}).
\end{aligned}
\tag{21}
$$

Again, the solution of this non-linear equation is approximated by applying an iterative procedure. Therefore, the steady state solutions for the cross-sectional area A are computed up to the numerical quadrature formula $\mathcal{Q}$ to approximate the integral of $R(x)$ and the iterative procedure to approximate the solution of (21).
Note that, in the case where $R(x) \equiv R$, we exactly recover the steady states defined by (18).

3. A fully well-balanced scheme for the blood flow equations with friction source term

Equipped with the steady states of system (7), we now derive a numerical scheme able to exactly preserve and capture this essential class of solutions. To address such an issue, we adopt a Godunov-type scheme. Therefore, for the sake of completeness, we first recall some generalities about Godunov-type schemes and, in particular, the construction of a Godunov-type scheme that uses an approximate Riemann solver with two intermediate states, see [14]. This approximate Riemann solver is then adapted to the blood flow equations with friction source term and the resulting numerical scheme is improved to ensure the preservation of all the steady states of system (7).

3.1. Generalities on Godunov-type schemes

Let us consider an hyperbolic system of conservation laws with source term, the so-called system of *balance laws*:

$$
\partial_t W + \partial_x F(W) = S(W), \tag{22}
$$

where W is the vector of unknowns, F is the flux function and S is the source term with, eventually, a space dependency. In order to approximate the solutions of (22), we first introduce the discretization of the one-dimensional space domain $\mathbb{R}$ by defining cells of constant volume Δx. The cell $I_i = (x_{i-\frac{1}{2}}, x_{i+\frac{1}{2}})$ has centre located in x_i, with $x_{i\pm\frac{1}{2}} = x_i \pm \Delta x/2$, for all $i \in \mathbb{Z}$. We discretize the time domain $\mathbb{R}^+$ by assuming a constant time step Δt, which is restricted according to the following Courant-Friedrichs-Lewy (CFL) stability condition:

$$
\frac{\Delta t}{\Delta x} \max_{i \in \mathbb{Z}} \left\{ |\lambda^L_{i+\frac{1}{2}}|, \, |\lambda^R_{i+\frac{1}{2}}| \right\} \leq \frac{1}{2}. \tag{23}
$$

where $\lambda^L_{i+\frac{1}{2}}$ and $\lambda^R_{i+\frac{1}{2}}$ are relevant approximations of the fastest wave characteristic velocities of the hyperbolic system, to be defined. At time t^n, the solution $W(x, t^n)$ of system (22) is approximated by a piecewise constant approximation, as follows:

$$
\widetilde{W}(x, t^n) = W_i^n, \quad \text{if } x \in (x_{i-\frac{1}{2}}, x_{i+\frac{1}{2}}), \tag{24}
$$

as depicted in Figure 2.

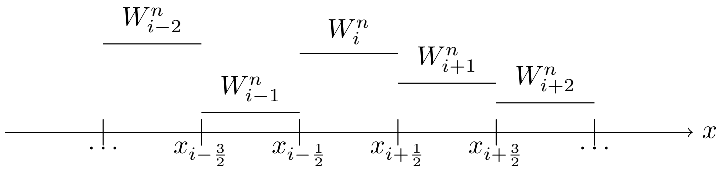

Figure 2: Piecewise constant approximate solution $\widetilde{W}(x, t^n)$.

In order to evolve in time this approximation and then to evaluate the updated states W_i^{n+1}, for all $i \in \mathbb{Z}$, we first adopt a Godunov's scheme formalism, according to [11], extended to deal with a source term. This numerical method is obtained by solving the system (22) endowed with the initial data $W(x, t = 0)$ given by (24). We denote by $\widetilde{W}_\Delta(x, t)$ the solution of this problem.
Since the approximate solution $\widetilde{W}(x, t^n)$ at time t^n is a piecewise constant function, each discontinuity in $\widetilde{W}(x, t^n)$ constitutes locally a Riemann problem, defined at each interface $x_{i+\frac{1}{2}}$ with the following initial data:

$$W(x - x_{i+\frac{1}{2}}, t = 0) = \begin{cases} W_i^n & \text{if } x < x_{i+\frac{1}{2}}, \\ W_{i+1}^n & \text{if } x > x_{i+\frac{1}{2}}. \end{cases} \tag{25}$$

Therefore, the solution of this initial-value problem can be expressed as the juxtaposition of the exact solutions to the local Riemann problems, as follows:

$$\widetilde{W}_\Delta(x, t) = W_{RP}\left(\frac{x - x_{i+1/2}}{t}; W_i^n, W_{i+1}^n\right), \quad \text{for } x \in (x_i, x_{i+1}), \quad t \in [0, \Delta t), \tag{26}$$

where $W_{RP}\left(\frac{x - x_{i+1/2}}{t}; W_i^n, W_{i+1}^n\right)$ denotes the exact solution to the Riemann problem with constant initial data W_i^n and W_{i+1}^n stated at the interface $x_{i+\frac{1}{2}}$. Moreover, by imposing the CFL condition (23), we ensure that there are no interactions between the waves from two neighbouring Riemann problems.
Finally, we define the updated approximate solution W_i^{n+1}, at time $t^{n+1} = t^n + \Delta t$ and within the cell I_i, by averaging $\widetilde{W}_\Delta(x, t^{n+1})$ as follows:

$$\begin{aligned} W_i^{n+1} &:= \frac{1}{\Delta x} \int_{x_{i-\frac{1}{2}}}^{x_{i+\frac{1}{2}}} \widetilde{W}_\Delta(x, t^{n+1})\, dx \\ &= \frac{1}{\Delta x} \int_0^{\frac{\Delta x}{2}} W_{RP}\left(\frac{x}{\Delta t}; W_{i-1}^n, W_i^n\right) dx + \frac{1}{\Delta x} \int_{-\frac{\Delta x}{2}}^0 W_{RP}\left(\frac{x}{\Delta t}; W_i^n, W_{i+1}^n\right) dx. \end{aligned} \tag{27}$$

As a consequence, the updated approximate solution is also piecewise constant on each cell and it is given by:

$$\widetilde{W}(x, t^{n+1}) = W_i^{n+1} \quad \text{if } x \in (x_{i-\frac{1}{2}}, x_{i+\frac{1}{2}}). \tag{28}$$

The resulting numerical scheme coincides with the well-known *Godunov's scheme* [11]. For the sake of completeness in the derivation of the updated states, let us emphasize that Godunov's scheme (27) recasts in a more usual form as follows:

$$
\begin{aligned}
W_i^{n+1} = W_i^n &- \frac{\Delta t}{\Delta x}\Big[\mathcal{F}(W_i^n, W_{i+1}^n) - \mathcal{F}(W_{i-1}^n, W_i^n)\Big] + \\
&+ \frac{\Delta t}{2}\Big[\overline{S}(W_{i-1}^n, W_i^n) + \overline{S}(W_i^n, W_{i+1}^n)\Big],
\end{aligned}
\tag{29}
$$

where $\mathcal{F}$ is the numerical flux function and $\overline{S}$ is the source term discretization, to be defined. Indeed, since the exact Riemann solution $W_{RP}\left(\frac{x}{t}; W_L, W_R\right)$ verifies (22), by integrating (22) over the control volume $\left[-\frac{\Delta x}{2}, \frac{\Delta x}{2}\right] \times [0, \Delta t]$, we get:

$$
\begin{aligned}
\frac{1}{\Delta x}\int_{-\frac{\Delta x}{2}}^{\frac{\Delta x}{2}} W_{RP}\left(\frac{x}{\Delta t}; W_L, W_R\right) dx = \frac{1}{2}(W_L + W_R) + \\
&- \frac{1}{\Delta x}\int_0^{\Delta t} F\left(W_{RP}\left(\frac{\Delta x}{2t}; W_L, W_R\right)\right) dt + \\
&+ \frac{1}{\Delta x}\int_0^{\Delta t} F\left(W_{RP}\left(-\frac{\Delta x}{2t}; W_L, W_R\right)\right) dt + \\
&+ \frac{\Delta t}{\Delta t \Delta x}\int_0^{\Delta t}\int_{-\frac{\Delta x}{2}}^{\frac{\Delta x}{2}} S\left(W_{RP}\left(\frac{x}{t}; W_L, W_R\right)\right) dx\, dt.
\end{aligned}
\tag{30}
$$

Next, we rewrite (27) as follows:

$$
\begin{aligned}
W_i^{n+1} &= \frac{1}{\Delta x}\int_{-\frac{\Delta x}{2}}^{\frac{\Delta x}{2}} \frac{1}{2}\left(W_{RP}\left(\frac{x}{\Delta t}; W_{i-1}^n, W_i^n\right) + W_{RP}\left(\frac{x}{\Delta t}; W_i^n, W_{i+1}^n\right)\right) dx + \\
&+ \frac{1}{\Delta x}\int_0^{\frac{\Delta x}{2}} \frac{1}{2}\left(W_{RP}\left(\frac{x}{\Delta t}; W_{i-1}^n, W_i^n\right) - W_{RP}\left(\frac{x}{\Delta t}; W_i^n, W_{i+1}^n\right)\right) dx + \\
&- \frac{1}{\Delta x}\int_{-\frac{\Delta x}{2}}^{0} \frac{1}{2}\left(W_{RP}\left(\frac{x}{\Delta t}; W_{i-1}^n, W_i^n\right) - W_{RP}\left(\frac{x}{\Delta t}; W_i^n, W_{i+1}^n\right)\right) dx.
\end{aligned}
\tag{31}
$$

Then, from (30) and enforcing the following continuity condition:

$$
\frac{1}{\Delta t}\int_0^{\Delta t} F\left(W_{RP}\left(\frac{\Delta x}{2t}; W_{i-1}^n, W_i^n\right)\right) dt = \frac{1}{\Delta t}\int_0^{\Delta t} F\left(W_{RP}\left(-\frac{\Delta x}{2t}; W_i^n, W_{i+1}^n\right)\right) dt,
\tag{32}
$$

we recover the scheme formulation (29), where we have set:

$$
\begin{aligned}
\mathcal{F}(W_L, W_R) = &\frac{\Delta x}{4\Delta t}(W_L - W_R) + \\
&+ \frac{1}{2\Delta t}\int_0^{\Delta t} F\left(W_{RP}\left(\frac{\Delta x}{2t}; W_L, W_R\right)\right) dt + \\
&+ \frac{1}{2\Delta t}\int_0^{\Delta t} F\left(W_{RP}\left(-\frac{\Delta x}{2t}; W_L, W_R\right)\right) dt + \\
&+ \frac{1}{2\Delta t}\int_0^{\frac{\Delta x}{2}} W_{RP}\left(\frac{x}{\Delta t}; W_L, W_R\right) dx + \\
&- \frac{1}{2\Delta t}\int_{-\frac{\Delta x}{2}}^{0} W_{RP}\left(\frac{x}{\Delta t}; W_L, W_R\right) dx
\end{aligned}
\tag{33}
$$

and

$$\overline{S}(W_L, W_R) = \frac{1}{\Delta t \Delta x} \int_0^{\Delta t} \int_{-\frac{\Delta x}{2}}^{\frac{\Delta x}{2}} S\left(W_{RP}\left(\frac{x}{t}; W_L, W_R\right)\right) dx\, dt. \tag{34}$$

Godunov's scheme is based on the knowledge of the exact solution of the Riemann problem arising between the piecewise constant approximations at the interfaces between two consecutive cells. In general, the exact Riemann solutions of (22) are not reachable. Indeed, the presence of source terms and non-linearities prevent the derivation of analytical exact solutions to Riemann problems. Therefore, in the framework of Godunov-type schemes, we are interested in introducing a consistent approximation of this exact solution. We denote by $\widetilde{W}_{RP}\left(\frac{x}{t}; W_L, W_R\right)$ the relevant approximation of the exact solution $W_{RP}\left(\frac{x}{t}; W_L, W_R\right)$ to the Riemann problem for system (22) between the two arbitrary states $W_L \in \Omega$ and $W_R \in \Omega$. Actually, this approximate solution can have a much simpler structure, as long as it does not violate the essential properties of conservation and consistency. Then, if the approximate Riemann solution $\widetilde{W}_{RP}$ is consistent with the integral form of (22), namely it satisfies the following consistency condition:

$$\frac{1}{\Delta x} \int_{-\frac{\Delta x}{2}}^{\frac{\Delta x}{2}} \widetilde{W}_{RP}\left(\frac{x}{t}; W_L, W_R\right) dx = \frac{1}{\Delta x} \int_{-\frac{\Delta x}{2}}^{\frac{\Delta x}{2}} W_{RP}\left(\frac{x}{t}; W_L, W_R\right) dx, \tag{35}$$

under the CFL condition (23), the solution updating formula (27) easily reformulates as follows:

$$W_i^{n+1} = \frac{1}{\Delta x} \int_0^{\frac{\Delta x}{2}} \widetilde{W}_{RP}\left(\frac{x}{\Delta t}; W_{i-1}^n, W_i^n\right) dx + \frac{1}{\Delta x} \int_{-\frac{\Delta x}{2}}^{0} \widetilde{W}_{RP}\left(\frac{x}{\Delta t}; W_i^n, W_{i+1}^n\right) dx, \tag{36}$$

to define the well-known *Godunov-type* scheme, according to the work by Harten *et al.* [14].

In conclusion, as soon as the approximate Riemann solver is known, the Godunov-type scheme is complete and fully determined. Then, the objective is to exhibit an approximate Riemann solver for the blood flow system (7), which ensures that the well-balanced property is satisfied by the resulting numerical scheme.

3.2. Derivation of a fully well-balanced approximate Riemann solver for the friction source term

We focus now on the derivation of a fully well-balanced approximate Riemann solver for the blood flow equations with friction source term (7).

To define the approximate solution $\widetilde{W}_{RP}$ to the Riemann problem, we adopt a two-state approximate Riemann solver, illustrated in Figure 3 and given by:

$$\widetilde{W}_{RP}\left(\frac{x}{t}; W_L, W_R\right) = \begin{cases} W_L & \text{if } x/t < \lambda_L, \\ W_L^* & \text{if } \lambda_L < x/t < 0, \\ W_R^* & \text{if } 0 < x/t < \lambda_R, \\ W_R & \text{if } x/t > \lambda_R, \end{cases} \tag{37}$$

where λ_L and λ_R denote suitable estimates for the fastest left and right wave velocities, respectively, and W_L^* and W_R^* are the two intermediate states to be described. In addition, in order to ensure that the crucial relation

$$\lambda_L < 0 < \lambda_R \tag{38}$$

holds, we choose a symmetric fan, by considering the following expressions of λ_L and λ_R:

$$\begin{cases} \lambda_L = \min(-|u_L| - c_L, -|u_R| - c_R, -\varepsilon_\lambda), \\ \lambda_R = \max(|u_L| + c_L, |u_R| + c_R, \varepsilon_\lambda), \end{cases} \tag{39}$$

where c is the sound speed given by (9) and ε_λ is a positive real constant to be fixed in the numerical applications. In fact, condition (38) ensures that the three waves with velocities λ_L, 0 and λ_R do not cross (sub-critical case).

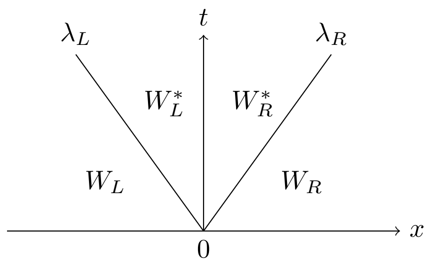

Figure 3: Structure of the two-state approximate Riemann solver with symmetric fan $\lambda_L < 0 < \lambda_R$.

Then, for such a choice of the Riemann solver, the approximate solution $\widetilde{W}_\Delta(x, t^n + t)$, depicted in Figure 4, for $0 < t < \Delta t$, when Δt is restricted by (9), and for $x \in (x_{i-\frac{1}{2}}, x_{i+\frac{1}{2}})$ is given by:

$$\forall i \in \mathbb{Z}, \quad \widetilde{W}_\Delta(x, t^n + t) = \begin{cases} W^{R,*}_{i-\frac{1}{2}} & \text{if } x \in \left[x_{i-\frac{1}{2}}, x_{i-\frac{1}{2}} + \lambda^R_{i-\frac{1}{2}} t\right], \\ W^n_i & \text{if } x \in \left[x_{i-\frac{1}{2}} + \lambda^R_{i-\frac{1}{2}} t, x_{i+\frac{1}{2}} + \lambda^L_{i+\frac{1}{2}} t\right], \\ W^{L,*}_{i+\frac{1}{2}} & \text{if } x \in \left[x_{i+\frac{1}{2}} + \lambda^L_{i+\frac{1}{2}} t, x_{i+\frac{1}{2}}\right]. \end{cases} \tag{40}$$

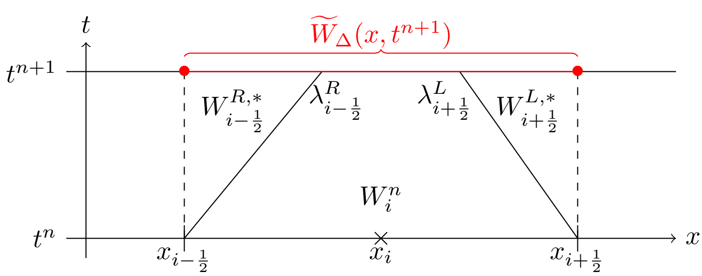

Figure 4: Full Godunov-type scheme using the two-state approximate Riemann solver.

At last, by using relation (36), we obtain the Godunov-type scheme under the following form:

$$W^{n+1}_i = W^n_i - \frac{\Delta t}{\Delta x}\left[\lambda^L_{i+\frac{1}{2}}(W^{L,*}_{i+\frac{1}{2}} - W^n_i) - \lambda^R_{i-\frac{1}{2}}(W^{R,*}_{i-\frac{1}{2}} - W^n_i)\right]. \tag{41}$$

We observe that, in order for W_i^{n+1} to be fully determined, we need to give explicit values to the intermediate states $W_{i+\frac{1}{2}}^{L,*}$ and $W_{i+\frac{1}{2}}^{R,*}$. As a consequence, we focus now on finding suitable definitions of the intermediate states for the blood flow system with friction source term. The resulting numerical scheme must be consistent and preserve all the steady states defined by (11) and (14), or by (19).

For the sake of simplicity, in the forthcoming scheme derivation we first adopt the blood flow system (7) with a constant viscous resistance $R > 0$.
Relevant definitions of the intermediate states $W_L^* = (A_L^*, q_L^*)^T$ and $W_R^* = (A_R^*, q_R^*)^T$ need to be obtained in order to fully determine the two-state approximate Riemann solver (37). Therefore, since we have four unknowns A_L^*, A_R^*, q_L^* and q_R^* to be defined, four equations are required. These equations will be derived by considering two essential properties that must be satisfied by the approximate Riemann solver: *consistency* with system (7) and *well-balancing*, i.e. preservation of all the steady states (11) and (14).
Concerning the issue of consistency, from (35) (see also [14]), we would like to impose the following integral consistency condition:

$$\frac{1}{\Delta x}\int_{-\frac{\Delta x}{2}}^{\frac{\Delta x}{2}} \widetilde{W}_{RP}\left(\frac{x}{\Delta t}; W_L, W_R\right) dx = \frac{1}{\Delta x}\int_{-\frac{\Delta x}{2}}^{\frac{\Delta x}{2}} W_{RP}\left(\frac{x}{\Delta t}; W_L, W_R\right) dx, \tag{42}$$

where the integral average of the exact Riemann solution is given by (30).
Now, it is worth noting that (30) turns out to be useless, since the exact Riemann solution can not be exhibited. As a consequence, we suggest to perform the following approximations:

$$\frac{1}{\Delta t}\int_0^{\Delta t} F\left(W_{RP}\left(-\frac{\Delta x}{2t}; W_L, W_R\right)\right) dt \approxeq F(W_L),$$

$$\frac{1}{\Delta t}\int_0^{\Delta t} F\left(W_{RP}\left(\frac{\Delta x}{2t}; W_L, W_R\right)\right) dt \approxeq F(W_R).$$

Moreover, we set:

$$\frac{1}{\Delta t \Delta x}\int_0^{\Delta t}\int_{-\frac{\Delta x}{2}}^{\frac{\Delta x}{2}} S\left(W_{RP}\left(\frac{x}{t}; W_L, W_R\right)\right) dx\, dt \approxeq \overline{S}, \tag{43}$$

where $\overline{S}$ denotes a suitable approximation of the source term, to be prescribed.
Equipped with these approximations, after straightforward computations, condition (42) rewrites as follows:

$$\begin{cases} \lambda_R(A_R^* - A_R) - \lambda_L(A_L^* - A_L) = (q_L - q_R)\,, \\ \lambda_R(q_R^* - q_R) - \lambda_L(q_L^* - q_L) = \left(\dfrac{q_L^2}{A_L} + \gamma A_L^{3/2} - \dfrac{q_R^2}{A_R} - \gamma A_R^{3/2}\right) + \Delta x \overline{S}. \end{cases} \tag{44}$$

To shorten the notations, we introduce the state $W_{HLL} = (A_{HLL}, q_{HLL})^T$, that is the well-known intermediate state of the HLL approximate Riemann solver (see [14]), defined by:

$$\begin{cases} (\lambda_R - \lambda_L)A_{HLL} = \lambda_R A_R - \lambda_L A_L - (q_R - q_L)\,, \\ (\lambda_R - \lambda_L)q_{HLL} = \lambda_R q_R - \lambda_L q_L - \left(\dfrac{q_R^2}{A_R} + \gamma A_R^{3/2} - \dfrac{q_L^2}{A_L} - \gamma A_L^{3/2}\right). \end{cases} \tag{45}$$

Then we get:

$$\begin{cases} \lambda_R A_R^* - \lambda_L A_L^* = (\lambda_R - \lambda_L) A_{HLL} \\ \lambda_R q_R^* - \lambda_L q_L^* = (\lambda_R - \lambda_L) q_{HLL} + \Delta x \overline{S}. \end{cases} \tag{46}$$

In order for the two-state approximate Riemann solver to be consistent with system (7), the four unknowns A_L^*, A_R^*, q_L^* and q_R^* and the additional source term average $\overline{S}$ need to satisfy relations (46).
At this point, we can tackle the issue of well-balancedness. Concerning the well-balanced property of the two-state approximate Riemann solver, we want to exhibit a sufficient condition for the preservation of a steady state solution of the blood flow system (7). More precisely, for a given pair $(A_{ref}, q_0) \in \Omega$, located at x_0, as soon as $(W_i^n)_{i\in\mathbb{Z}}$ verifies for all $i \in \mathbb{Z}$

$$\begin{cases} q_i^n = q_0, \\ -(q_i^n)^2 \log A_i^n + \dfrac{3}{5}\gamma (A_i^n)^{5/2} + R q_i^n x_i = -q_0^2 \log A_{ref} + \dfrac{3}{5}\gamma A_{ref}^{5/2} + R q_0 x_0, \end{cases} \tag{47}$$

we expect a steady solution defined by $W_i^{n+1} = W_i^n$, for all $i \in \mathbb{Z}$.
Then, from scheme (41), we clearly see that the solution is stationary if we have:

$$\forall i \in \mathbb{Z}, \quad W_{i+\frac{1}{2}}^{L,*} = W_i^n \quad \text{and} \quad W_{i-\frac{1}{2}}^{R,*} = W_i^n. \tag{48}$$

Hence, the approximate Riemann solver should be stationary, namely $W_L^* = W_L$ and $W_R^* = W_R$, as soon as W_L and W_R define a steady state (*Well-Balanced Principle*).
In particular, according to the steady state system (10), two consecutive states W_L and W_R are at equilibrium and locally define a steady state if and only if they satisfy the following relations:

$$\begin{cases} q_L = q_R = q_0, \\ -q_0^2 \log A_R + \dfrac{3}{5}\gamma A_R^{5/2} + q_0^2 \log A_L - \dfrac{3}{5}\gamma A_L^{5/2} = -R\, q_0 \Delta x. \end{cases} \tag{49}$$

Equipped with the above Well-Balanced Principle, we are now able to provide a necessary condition to be satisfied by the source term discretization $\overline{S}$, in order to preserve the steady states. The following result holds.

Lemma 1. *Let W_L and W_R be given in Ω such that they define a steady state, namely relations (49) are satisfied. Then, to preserve $W_L^* = W_L$ and $W_R^* = W_R$, necessarily we have:*

$$\overline{S} = -\left(\frac{-q_0^2 \dfrac{A_R - A_L}{A_L A_R} + \gamma \left(A_R^{3/2} - A_L^{3/2} \right)}{-q_0^2 \left(\log A_R - \log A_L \right) + \dfrac{3}{5}\gamma \left(A_R^{5/2} - A_L^{5/2} \right)} \right) R\, q_0. \tag{50}$$

Proof. Since a steady state verifies (49), we have $q_L = q_R = q_0$. Imposing $W_L^* = W_L$ and $W_R^* = W_R$ yields:

$$\Delta x \overline{S} = \left(\frac{q_0^2}{A_R} + \gamma A_R^{3/2} \right) - \left(\frac{q_0^2}{A_L} + \gamma A_L^{3/2} \right).$$

By introducing the jump function $[\cdot]$ as $[x] = (x_R - x_L)$, the above relation can be rewritten as follows:

$$\Delta x \overline{S} = -q_0^2 \frac{[A]}{A_L A_R} + \gamma \frac{[A^{3/2}]}{[A]}[A] = \left(-\frac{q_0^2}{A_L A_R} + \gamma \frac{[A^{3/2}]}{[A]} \right) [A]. \tag{51}$$

Analogously, we can rewrite the steady state relation (49) in terms of the jump function, as follows:

$$-Rq_0\Delta x = -q_0^2[\log A] + \frac{3}{5}\gamma[A^{\frac{5}{2}}] = \left(-q_0^2\frac{[\log A]}{[A]} + \frac{3}{5}\gamma\frac{[A^{5/2}]}{[A]}\right)[A]. \tag{52}$$

Then, from relation (52), we can easily exhibit an expression for $[A] = A_R - A_L$, given by:

$$[A] = -\frac{R\,q_0\Delta x}{\left(-q_0^2\frac{[\log A]}{[A]} + \frac{3}{5}\gamma\frac{[A^{5/2}]}{[A]}\right)}.$$

Finally, we substitute the above expression of $[A]$ into (51), to obtain, after straightforward computations, the expected formula (50) to be satisfied by $\overline{S}$. The proof is then achieved. □

As a consequence, since from Lemma 1 the source term discretization $\overline{S}$ must coincide with (50) as long as W_L and W_R verify relations (49), we adopt the following definition of $\overline{S}$:

$$\overline{S} = -\left(\frac{-\overline{q}_{LR}^2\dfrac{A_R - A_L}{A_L A_R} + \gamma\left(A_R^{3/2} - A_L^{3/2}\right)}{-\overline{q}_{LR}^2\left(\log A_R - \log A_L\right) + \dfrac{3}{5}\gamma\left(A_R^{5/2} - A_L^{5/2}\right)}\right) R\,\overline{q}_{LR}, \tag{53}$$

where $\overline{q}_{LR} := \overline{q}_{LR}(q_L, q_R)$ stands for a suitable average of the discharge q such that $\overline{q}_{LR}(q, q) = q$. In this work, we select the following average:

$$\overline{q}_{LR}(q_L, q_R) := \frac{q_L + q_R}{2}. \tag{54}$$

This average indeed ensures that, if $q_L = q_R$, then $\overline{q}_{LR} = q_L = q_R$. In particular, if a steady state is considered, then we have $q_L = q_R = q_0$; hence, $\overline{q}_{LR} = q_0$ in this case.
Now, we emphasize that the adopted formula (53) is a consistent discretization with the source term $S(W) = -R\,q/A$.

Lemma 2. *Let $\overline{S}$ be given by (53). Let $(A, q) : \mathbb{R} \to \Omega$ be given smooth. Let us consider $(A_L, q_L) = (A(x - \Delta x), q(x - \Delta x))$ and $(A_R, q_R) = (A(x + \Delta x), q(x + \Delta x))$. Then, we have:*

$$\lim_{\Delta x \to 0} \overline{S} = -R\,\frac{q}{A}. \tag{55}$$

Proof. The following sequence of equalities holds:

$$\begin{aligned}\lim_{\Delta x \to 0} \overline{S} &= \lim_{\Delta x \to 0} -\left(\frac{\dfrac{-\overline{q}_{LR}^2}{A_L A_R} + \gamma\dfrac{A_R^{3/2} - A_L^{3/2}}{A_R - A_L}}{-\overline{q}_{LR}^2\dfrac{\log A_R - \log A_L}{A_R - A_L} + \dfrac{3}{5}\gamma\dfrac{A_R^{5/2} - A_L^{5/2}}{A_R - A_L}}\right) R\,\overline{q}_{LR}(q_L, q_R)\\ &= -\left(\frac{-q^2/A^2 + \dfrac{3}{2}\gamma A^{1/2}}{-q^2/A + \dfrac{3}{2}\gamma A^{3/2}}\right) R\,q\\ &= -R\,\frac{q}{A},\end{aligned}$$

and the proof is then achieved. □

Next, equipped with the expression of $\overline{S}$, we focus on the definition of the intermediate states $(A_L^*, q_L^*)^T$ and $(A_R^*, q_R^*)^T$. We have already obtained that these four unknowns must satisfy the consistency relations (46), but clearly two equations are still missing to solve this problem. Therefore, we suggest to adopt suitable extensions of the steady state conditions (49).
Concerning the discharge, we propose to adopt:

$$q_L^* = q_R^* = q^*, \tag{56}$$

so that, arguing (46), we immediately get:

$$q^* = q_{HLL} + \frac{\Delta x}{\lambda_R - \lambda_L}\overline{S}. \tag{57}$$

Thereafter, we have to define the intermediate cross-sectional areas A_L^* and A_R^*, in order to complete W_L^* and W_R^*. From (46), recall that we have:

$$\lambda_R A_R^* - \lambda_L A_L^* = (\lambda_R - \lambda_L) A_{HLL}. \tag{58}$$

Moreover, A_L^* and A_R^* have to be chosen so as to ensure that W_L^* and W_R^* satisfy the Well-Balanced Principle. If W_L and W_R define a steady state, then, from (49), the following relation is satisfied:

$$\mathcal{E}(A_L, A_R) = -Rq_0\Delta x, \tag{59}$$

where we have introduced the following function:

$$\mathcal{E}(A_L, A_R) = -\overline{q}_{LR}^2 \log A_R + \frac{3}{5}\gamma A_R^{5/2} + \overline{q}_{LR}^2 \log A_L - \frac{3}{5}\gamma A_L^{5/2}, \tag{60}$$

and, under the hypothesis $q_L = q_R = q_0$, we have $\overline{q}_{LR}(q_L, q_R) = q_0$.
Since equation (60) is strongly non-linear, it is not reasonable to adopt, together with (58), the condition $\mathcal{E}(A_L^*, A_R^*) = -R\,\overline{q}_{LR}\Delta x$ to complete the system for the unknowns A_L^* and A_R^*. As a consequence, we suggest to consider some suitable linearization $\mathcal{L}$ of the function $\mathcal{E}$, in order to easily solve the following linear system in the unknowns A_L^* and A_R^*:

$$\begin{cases} \lambda_R A_R^* - \lambda_L A_L^* = (\lambda_R - \lambda_L) A_{HLL}, \\ \mathcal{L}(\mathcal{E}(A_L^*, A_R^*)) = -R\,\overline{q}_{LR}\Delta x. \end{cases} \tag{61}$$

Several linearizations of $\mathcal{E}$ can be employed. Here, we choose $\mathcal{L}$ given by:

$$\mathcal{L}(\mathcal{E}(A_L^*, A_R^*)) = \mathcal{E}(A_L, A_R) + \nabla\mathcal{E}(A_L, A_R) \cdot \begin{pmatrix} A_L^* - A_L \\ A_R^* - A_R \end{pmatrix}. \tag{62}$$

We solve the linear system (61) and straightforward computations yield the full formulas for the intermediate cross-sectional areas A_L^* and A_R^*:

$$\begin{cases} A_L^* = \dfrac{\overline{q}_{LR}^2 \log\left(\dfrac{A_R}{A_L}\right) + \dfrac{9}{10}\gamma\left(A_R^{5/2} - A_L^{5/2}\right) + \dfrac{\lambda_R - \lambda_L}{\lambda_R}\left(\dfrac{\overline{q}_{LR}^2}{A_R} - \dfrac{3}{2}\gamma A_R^{3/2}\right) A_{HLL} - R\,\overline{q}_{LR}\Delta x}{\left(\dfrac{\overline{q}_{LR}^2}{A_L} - \dfrac{\lambda_L}{\lambda_L\lambda_R}\overline{q}_{LR}^2 + \dfrac{3}{2}\gamma\dfrac{\lambda_L}{\lambda_R}A_R^{3/2} - \dfrac{3}{2}\gamma A_L^{3/2}\right)}, \\ A_R^* = \dfrac{\lambda_L}{\lambda_R}A_L^* + \dfrac{\lambda_R - \lambda_L}{\lambda_R}A_{HLL}, \end{cases} \tag{63}$$

where $\overline{q}_{LR}$ is still given by (54).
As soon as also A_L^* and A_R^* are known, the intermediate states W_L^* and W_R^* are fully determined, and, together with the numerical source term $\overline{S}$, they ensure the consistency and the well-balanced properties of the approximate Riemann solver.

Equipped with the intermediate states W_L^* and W_R^* of the approximate Riemann solver and the source term discretization $\overline{S}$, scheme (41) is complete.
To achieve the scheme presentation, let us underline that the numerical method (41) may be given in a usual flux formulation. Indeed, after straightforward computations, the following result holds.

Lemma 3. *The scheme (41) can be rewritten under the following form:*

$$W_i^{n+1} = W_i^n - \frac{\Delta t}{\Delta x}\left[\mathcal{F}_{i+\frac{1}{2}}^n - \mathcal{F}_{i-\frac{1}{2}}^n\right] + \frac{\Delta t}{2}\left[\mathcal{S}_{i+\frac{1}{2}}^n + \mathcal{S}_{i-\frac{1}{2}}^n\right], \tag{64}$$

with

$$\begin{aligned}\mathcal{F}_{i+\frac{1}{2}}^n = &\frac{1}{2}\left[F(W_i^n) + F(W_{i+1}^n)\right] + \\ &+ \frac{1}{2}\lambda_{i+\frac{1}{2}}^L\left(W_{i+\frac{1}{2}}^{L,*} - W_i^n\right) + \frac{1}{2}\lambda_{i+\frac{1}{2}}^R\left(W_{i+\frac{1}{2}}^{R,*} - W_{i+1}^n\right)\end{aligned} \tag{65}$$

and

$$\mathcal{S}_{i+\frac{1}{2}}^n = \begin{pmatrix} 0 \\ \overline{S}\left(A_i^n, A_{i+1}^n, \overline{q}_{i+\frac{1}{2}}, \Delta x\right)\end{pmatrix}, \tag{66}$$

where $\mathcal{F}_{i+\frac{1}{2}}^n$ is the numerical flux function *computed at the interface $x_{i+\frac{1}{2}}$, and $\mathcal{S}_{i+\frac{1}{2}}^n$ is the* numerical source term *computed at the interface $x_{i+\frac{1}{2}}$. In particular, in (66), the discretization $\overline{S}$ is given by (53) and $\overline{q}_{i+\frac{1}{2}} = \overline{q}_{LR}(q_i^n, q_{i+1}^n)$.*

We omit the proof of this statement since it is a direct extension of the formulation (29), when adopting the derived approximate Riemann solver.

To conclude this section, we extend the obtained fully well-balanced scheme to the generalized model with variable viscous resistance $R(x)$. According to (19), two consecutive states W_L and W_R locally define a steady state if and only if they satisfy the following relations:

$$\begin{cases} q_L = q_R = q_0, \\ \mathcal{F}_{q_0}(A_R) - \mathcal{F}_{q_0}(A_L) = -q_0 \displaystyle\int_{x_L}^{x_R} R(x)\,dx, \end{cases} \tag{67}$$

where the function $\mathcal{F}_{q_0}$ is given by (16). The integral of the function $R(x)$ between x_L and x_R in (67) is approximated by a quadrature formula to be chosen suitably and we denote it by:

$$\mathcal{Q}(R, x_L, x_R) \approx \int_{x_L}^{x_R} R(x)\,dx. \tag{68}$$

Let us now derive the new source term discretization $\overline{S}$. We prove the following result.

Lemma 4. *Let W_L and W_R be given in Ω such that relations (67) are satisfied. Then, to preserve $W_L^* = W_L$ and $W_R^* = W_R$, necessarily we have:*

$$\Delta x \overline{S} = \left(\frac{\mathcal{Q}_0^2(A_L, A_R, q_0, R)}{A_L A_R} - \gamma \frac{A_R^{3/2} - A_L^{3/2}}{A_R - A_L} \right) \left(\frac{A_R - A_L}{\mathcal{F}_{q_0}(A_R) - \mathcal{F}_{q_0}(A_L)} \right) q_0 \mathcal{Q}(R, x_L, x_R), \tag{69}$$

where we have set:

$$\mathcal{Q}_0^2(A_L, A_R, q_0, R) := \frac{\frac{3}{5}\gamma(A_R^{5/2} - A_L^{5/2}) + q_0 \mathcal{Q}(R, x_L, x_R)}{\log(A_R/A_L)}.$$

Proof. From the second steady state relation in (67), we first evaluate the quantity q_0^2 as follows:

$$q_0^2 = \frac{\frac{3}{5}\gamma(A_R^{5/2} - A_L^{5/2}) + q_0 \mathcal{Q}(R, x_L, x_R)}{\log(A_R/A_L)} =: \mathcal{Q}_0^2(A_L, A_R, q_0, R). \tag{70}$$

Now, we recall that the intermediate states W_L^* and W_R^* have to verify the consistency relations (46). Since W_L and W_R define a steady state, by imposing $W_L^* = W_L$ and $W_R^* = W_R$, the second consistency relation in (46) becomes:

$$\Delta x \overline{S} = q_0^2 \left(\frac{1}{A_R} - \frac{1}{A_L} \right) + \gamma \left(A_R^{3/2} - A_L^{3/2} \right). \tag{71}$$

Then, by replacing expression (70) for q_0^2 found above, we get:

$$\Delta x \overline{S} = \mathcal{Q}_0^2(A_L, A_R, q_0, R) \left(\frac{1}{A_R} - \frac{1}{A_L} \right) + \gamma \left(A_R^{3/2} - A_L^{3/2} \right). \tag{72}$$

Moreover, from (67), we exhibit the following quantity:

$$[A] = (A_R - A_L) = -\left(\frac{A_R - A_L}{\mathcal{F}_{q_0}(A_R) - \mathcal{F}_{q_0}(A_L)} \right) q_0 \mathcal{Q}(R, x_L, x_R). \tag{73}$$

Finally, we substitute the above expression of $[A]$ into (72), to obtain, after straightforward computations, the expected formula (69) to be satisfied by $\overline{S}$. This concludes the proof. □

Once again, since from Lemma 4 we have that the source term discretization $\overline{S}$ must coincide with (69) as long as W_L and W_R satisfy relations (67), we adopt the following definition of $\overline{S}$:

$$\Delta x \overline{S} = \left(\frac{\mathcal{Q}_0^2(A_L, A_R, \overline{q}_{LR}, R)}{A_L A_R} - \gamma \frac{A_R^{3/2} - A_L^{3/2}}{A_R - A_L} \right) \left(\frac{A_R - A_L}{\mathcal{F}_{\overline{q}_{LR}}(A_R) - \mathcal{F}_{\overline{q}_{LR}}(A_L)} \right) \overline{q}_{LR} \mathcal{Q}(R, x_L, x_R), \tag{74}$$

with $\overline{q}_{LR}$ being defined as in (54). This definition is consistent with the friction source term $S(W) = -R(x)\, q/A$.

The intermediate states W_L^* and W_R^* of the two-state approximate Riemann solver are then determined by enforcing the same conditions as for the system with constant viscous resistance. In particular, the intermediate discharge q^* is given by:

$$q_L^* = q_R^* = q^* = q_{HLL} + \frac{\Delta x}{\lambda_R - \lambda_L} \overline{S}, \tag{75}$$

while the intermediate cross-sectional areas A_L^* and A_R^* are solution of the following linearized system:

$$\begin{cases} \lambda_R A_R^* - \lambda_L A_L^* = (\lambda_R - \lambda_L) A_{HLL}, \\ \mathcal{L}(\mathcal{E}(A_L^*, A_R^*)) = -\overline{q}_{LR} \mathcal{Q}(R, x_L, x_R), \end{cases} \tag{76}$$

where the linearization $\mathcal{L}$ is given by (62).

Finally, we have to check that, if W_L, W_R and $R(x)$ are given at equilibrium, then this implies $W_L^* = W_L$ and $W_R^* = W_R$. Under steady state, straightforward computations yield $q^* = q_0$. In addition, we can plainly see that a natural solution of system (76) is given by $A_L^* = A_L$ and $A_R^* = A_R$. As a consequence, since the linear system admits a unique solution, $A_L^* = A_L$ and $A_R^* = A_R$ is the only solution.

4. Properties satisfied by the fully well-balanced scheme

In Section 3, we have constructed the intermediate states (57) and (63) and defined the source term discretization (53), which determine a consistent and fully well-balanced two-state approximate Riemann solver. However, from formulas (63) we can clearly see that we have no guarantee that the intermediate cross-sectional areas A_L^* and A_R^* remain positive, but they can become zero or even negative. If that is the case, then (41) can yield a negative updated cross-sectional area A_i^{n+1}, which means that the updated state W_i^{n+1} would not belong any more to the admissible states space Ω. Then, in order to recover and preserve a physically admissible solution, we apply the following procedure (see for instance [16, 17]). It consists in enforcing the positivity of A_L^* and A_R^*, but still ensuring that they satisfy the consistency relation (46). For the sake of simplicity, this procedure is described here in the case of constant viscous resistance $R > 0$, but the same argument holds also in the case of variable viscous resistance $R(x)$.

We introduce a positive parameter $\varepsilon > 0$ that controls the positivity of A_L^* and A_R^*, namely we want $A_L^* \geq \varepsilon > 0$ and $A_R^* \geq \varepsilon > 0$. For given states W_L and W_R, we select the parameter $\varepsilon > 0$ such that

$$\varepsilon = \min(A_L, A_R, A_{HLL}). \tag{77}$$

Since $A_L > 0$, $A_R > 0$ and $A_{HLL} > 0$, hence also $\varepsilon > 0$. If $A_L^* < \varepsilon$, then we fix $A_L^* = \varepsilon$ and we choose A_R^* according to the first consistency condition in (46), which ensures $A_R^* > 0$. On the other hand, in the same way, if $A_R^* < \varepsilon$, then we take $A_R^* = \varepsilon$ and we compute A_L^* according to the first relation in (46), which guarantees $A_L^* > 0$. Then, the new intermediate states $W_L^* = (A_L^{**}, q_L^*)^T$ and $W_R^* = (A_R^{**}, q_R^*)^T$ of the two-state approximate Riemann solver are given by:

$$\begin{cases} q_L^* = q_R^* = q^* = q_{HLL} + \dfrac{\Delta x}{\lambda_R - \lambda_L} \overline{S}, \\ A_L^{**} = \min\left\{ \max\left\{A_L^*, \varepsilon\right\}, \dfrac{\lambda_R}{\lambda_L}\varepsilon + \left(1 - \dfrac{\lambda_R}{\lambda_L}\right) A_{HLL} \right\}, \\ A_R^{**} = \min\left\{ \max\left\{A_R^*, \varepsilon\right\}, \dfrac{\lambda_L}{\lambda_R}\varepsilon + \left(1 - \dfrac{\lambda_L}{\lambda_R}\right) A_{HLL} \right\}, \end{cases} \tag{78}$$

which always yield $A_L^{**} \geq \varepsilon > 0$ and $A_R^{**} \geq \varepsilon > 0$. This correction procedure is illustrated in Figure 5.

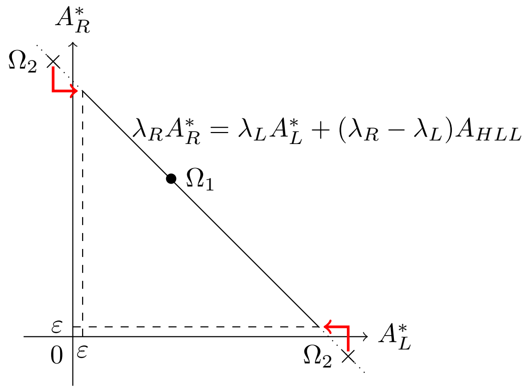

Figure 5: Correction procedure to ensure positiveness and consistency of the intermediate cross-sectional areas A_L^* and A_R^*. The line represents the first consistency relation (46) in the $A_L^* - A_R^*$ half-plane. If the point (A_L^*, A_R^*) belongs to domain Ω_1, then A_L^* and A_R^* are not modified. On the other hand, if (A_L^*, A_R^*) corresponds to a point within domain Ω_2, we replace (A_L^*, A_R^*) according to (46), namely by applying definitions (78).

As a consequence, by applying this positivity correction and by substituting the expressions (63) of A_L^* and A_R^* with the new expressions in (78), we have that the cross-sectional area A never vanishes and its positiveness is preserved.
In the following, we present now two important results, which sum up the properties we have obtained so far, for the two-state approximate Riemann solver and the full numerical scheme.

Lemma 5. *Assume $\varepsilon > 0$ such that (77) is fulfilled. Then, the intermediate states $W_L^* = (A_L^{**}, q^*)^T$ and $W_R^* = (A_R^{**}, q^*)^T$ given by (78) satisfy the following properties:*

(i) consistency: the quantities A_L^{**}, A_R^{**} and $q_L^* = q_R^* = q^*$ satisfy equations (46);

(ii) positivity preservation: if $A_L > 0$, $A_R > 0$ and $A_{HLL} > 0$, then $A_L^{**} \geq \varepsilon > 0$ and $A_R^{**} \geq \varepsilon > 0$;

(iii) well-balancing: $W_L^* = W_L$ and $W_R^* = W_R$ as soon as W_L and W_R define a steady state.

Proof. Since ε is defined by (77), property *(ii)* is obviously satisfied. Indeed, as stated in (78), A_L^{**} and A_R^{**} stand for the minimum of quantities that are greater than or equal to ε, which is a strictly positive parameter.
Concerning the consistency property *(i)*, since the second relation in (46) is obviously satisfied by q^*, by construction, then property *(i)* is established as soon as we prove that also A_L^{**} and A_R^{**} satisfy the first equation in (46), namely:

$$\lambda_R A_R^{**} - \lambda_L A_L^{**} = (\lambda_R - \lambda_L) A_{HLL}. \tag{79}$$

Let us assume that $|\lambda_L|$ and $|\lambda_R|$ are chosen large enough so that to ensure $A_{HLL} > 0$, with $\lambda_L < 0 < \lambda_R$. Indeed, from the definition of A_{HLL} in (45) and definitions (39) of the wave speed estimates λ_L and λ_R, we obtain:

$$A_{HLL} = \frac{1}{2}(A_L + A_R) - \frac{1}{2\lambda}(q_R - q_L),$$

where we have set $\lambda = \lambda_R = -\lambda_L > 0$, and we can plainly see that it is always possible to select a value of λ large enough to get $A_{HLL} \approxeq \frac{1}{2}(A_L + A_R) > 0$. Then, from formulas (78) we have three possible configurations:

- if both $A_L^* \geq \varepsilon$ and $A_R^* \geq \varepsilon$, with A_L^* and A_R^* given by (63), then $A_L^{**} = A_L^*$ and $A_R^{**} = A_R^*$;
- if $A_L^* < \varepsilon$, then $A_L^{**} = \varepsilon$ and $A_R^{**} = \dfrac{\lambda_L}{\lambda_R}\varepsilon + \left(1 - \dfrac{\lambda_L}{\lambda_R}\right) A_{HLL}$;
- if $A_R^* < \varepsilon$, then $A_R^{**} = \varepsilon$ and $A_L^{**} = \dfrac{\lambda_R}{\lambda_L}\varepsilon + \left(1 - \dfrac{\lambda_R}{\lambda_L}\right) A_{HLL}$.

By straightforward computations, we easily obtain that in all cases the consistency relation (79) systematically holds and the consistency property *(i)* is then proved.
What is left to check now is that the positivity preserving procedure stated in (78) does not affect the well-balanced property of the approximate Riemann solver. In order to prove the well-balancedness, let us assume that W_L and W_R define a steady state, namely:

$$\begin{cases} q_L = q_R = q_0 \\ \mathcal{E}(A_L, A_R) = -Rq_0\Delta x, \end{cases} \tag{80}$$

where the function $\mathcal{E}$ is given by (60), and we want to prove that $W_L^* = W_L$ and $W_R^* = W_R$. Let us start with q^*. At the steady state, the following chain of equalities holds:

$$\begin{aligned} q^* &= \frac{\lambda_R q_0 - \lambda_L q_0}{\lambda_R - \lambda_L} - \frac{F^q(W_R) - F^q(W_L)}{\lambda_R - \lambda_L} + \frac{\Delta x}{\lambda_R - \lambda_L}\overline{S} \\ &= q_0 - \frac{1}{\lambda_R - \lambda_L}\left(F^q(W_R) - F^q(W_L) - \Delta x\overline{S}\right) \\ &= q_0, \end{aligned} \tag{81}$$

where, in the last step, we have used the fact that at the steady state $\Delta x\overline{S} = (F^q(W_R) - F^q(W_L))$. Afterwards, we have to prove that also $A_L^{**} = A_L$ and $A_R^{**} = A_R$. In order to show these equalities, we proceed as follows: we first prove that at equilibrium $A_L^* = A_L$ and $A_R^* = A_R$; next, we verify that at steady state the only case possible is $A_L^{**} = A_L^*$ and $A_R^{**} = A_R^*$, so that we obtain $A_L^{**} = A_L^* = A_L$ and $A_R^{**} = A_R^* = A_R$, and thus property *(iii)* holds. Since at equilibrium we have $q_L = q_R = q_0$, from (63) we get:

$$A_R^* = A_R + \frac{\lambda_L}{\lambda_R}(A_L^* - A_L). \tag{82}$$

Moreover, the expression for A_L^* in (63) becomes:

$$\begin{aligned} A_L^* &= \frac{\frac{3}{2}\gamma(A_R^{5/2} - A_L^{5/2}) + \left(\frac{\lambda_R A_R - \lambda_L A_L}{\lambda_R}\right)\left(\frac{q_0^2}{A_R} - \frac{3}{2}\gamma A_R^{3/2}\right)}{\left(\frac{q_0^2}{A_L} - \frac{\lambda_L}{\lambda_R A_R}q_0^2 + \frac{3}{2}\gamma\frac{\lambda_L}{\lambda_R}A_R^{3/2} - \frac{3}{2}\gamma A_L^{3/2}\right)} \\ &= \frac{\left(q_0^2 - \frac{\lambda_L A_L}{\lambda_R A_R}q_0^2 + \frac{3}{2}\gamma\frac{\lambda_L}{\lambda_R}A_L A_R^{3/2} - \frac{3}{2}\gamma A_L^{5/2}\right)}{\left(\frac{q_0^2}{A_L} - \frac{\lambda_L}{\lambda_R A_R}q_0^2 + \frac{3}{2}\gamma\frac{\lambda_L}{\lambda_R}A_R^{3/2} - \frac{3}{2}\gamma A_L^{3/2}\right)} \\ &= A_L, \end{aligned} \tag{83}$$

and then, using this result into (82) yields also:

$$A_R^* = A_R. \tag{84}$$

As last step of the proof, we have to show that under steady state we always have $A_L^{**} = A_L^*$ and $A_R^{**} = A_R^*$. Let us start by A_L^{**}. From (78), by using the result obtained in (83) and definition (77) of ε, at equilibrium we obtain that A_L^{**} is defined as follows:

$$A_L^{**} = \min\left\{A_L, \frac{\lambda_R}{\lambda_L}\varepsilon + \left(1 - \frac{\lambda_R}{\lambda_L}\right) A_{HLL}\right\}.$$

Therefore, in order to prove that $A_L^{**} = A_L^* = A_L$, we have to check that:

$$\min\left\{A_L, \frac{\lambda_R}{\lambda_L}\varepsilon + \left(1 - \frac{\lambda_R}{\lambda_L}\right) A_{HLL}\right\} = A_L,$$

namely that

$$A_L \leq \frac{\lambda_R}{\lambda_L}\varepsilon + \left(1 - \frac{\lambda_R}{\lambda_L}\right) A_{HLL}. \tag{85}$$

By expanding the expression of A_{HLL} and using the fact that $\lambda_L < 0 < \lambda_R$, it is easy to see that the above inequality is always satisfied and then $A_L^{**} = A_L$.
Similar computations lead to $A_R^{**} = A_R$.
This proves the well-balanced property *(iii)*, which means that $W_L^* = W_L$ and $W_R^* = W_R$ as soon as W_L and W_R define a steady state. Then, the proof is achieved and Lemma 5 is established. □

Equipped with Lemma 5, we can now state the following result concerning the full numerical scheme (41).

Lemma 6. *Consider $W_i^n \in \Omega$ for all $i \in \mathbb{Z}$, where Ω is the admissible states space defined as follows:*

$$\Omega = \left\{W = (A, q)^T \in \mathbb{R}^2 : A > 0,\, q \in \mathbb{R}\right\} \subset \mathbb{R}^2.$$

Assume that the intermediate states $W_{i+\frac{1}{2}}^{L,*}$ and $W_{i+\frac{1}{2}}^{R,*}$ of the two-state approximate Riemann solver are given, for all $i \in \mathbb{Z}$, by:

$$W_{i+\frac{1}{2}}^{L,*} = \begin{pmatrix} A_L^{**}(W_i^n, W_{i+1}^n) \\ q^*(W_i^n, W_{i+1}^n) \end{pmatrix} \quad \text{and} \quad W_{i+\frac{1}{2}}^{R,*} = \begin{pmatrix} A_R^{**}(W_i^n, W_{i+1}^n) \\ q^*(W_i^n, W_{i+1}^n) \end{pmatrix},$$

where A_L^{**}, A_R^{**} and q^* are given by (78). Assume also $\varepsilon > 0$ given by (77). Then, the resulting Godunov-type scheme, given by (41) under the CFL stability condition (23), satisfies the following properties:

(1) consistency with the blood flow system (7);

(2) positivity preservation: $W_i^{n+1} \in \Omega$ for all $i \in \mathbb{Z}$;

(3) well-balancing: if $(W_i^n)_{i\in\mathbb{Z}}$ defines a steady state, then for all $i \in \mathbb{Z}$, $W_i^{n+1} = W_i^n$.

Proof. The consistency property *(1)* is a direct consequence of Lemma 5.
Concerning the positivity preservation *(2)*, we have to prove that $\forall i \in \mathbb{Z}$, $A_i^{n+1} > 0$ as soon as $A_i^n > 0$. From Lemma 5, we have $A_{i+\frac{1}{2}}^{L,*} \geq \varepsilon_i^n$ and $A_{i+\frac{1}{2}}^{R,*} \geq \varepsilon_i^n$, with

$\varepsilon_i^n = \min(A_i^n, A_{i+1}^n, A_{i+\frac{1}{2}}^{HLL})$ and $A_{i+\frac{1}{2}}^{HLL}$ given by evaluating the HLL intermediate state (45) between W_i^n and W_{i+1}^n. Then, from the Godunov-type scheme (41), the updated cross-sectional area A_i^{n+1} can be rewritten as follows:

$$
\begin{aligned}
A_i^{n+1} = {} & A_i^n \left(1 + \frac{\Delta t}{\Delta x}\lambda_{i+\frac{1}{2}}^L - \frac{\Delta t}{\Delta x}\lambda_{i-\frac{1}{2}}^R\right) + \\
& - A_{i+\frac{1}{2}}^{L,*}\left(\frac{\Delta t}{\Delta x}\lambda_{i+\frac{1}{2}}^L\right) + A_{i-\frac{1}{2}}^{R,*}\left(\frac{\Delta t}{\Delta x}\lambda_{i-\frac{1}{2}}^R\right).
\end{aligned}
\tag{86}
$$

We assume that $A_i^n > 0$. Recall that $\lambda_{i+\frac{1}{2}}^L < 0$ and $\lambda_{i-\frac{1}{2}}^R > 0$ under (38) and recall also the CFL condition (23), which constraints the time step Δt. As a consequence, we have:

$$
\frac{\Delta t}{\Delta x}|\lambda_{i+\frac{1}{2}}^L| \leq \frac{1}{2} \quad \text{and} \quad \frac{\Delta t}{\Delta x}\lambda_{i-\frac{1}{2}}^R \leq \frac{1}{2}.
$$

Therefore, from the above assumptions, the following inequality holds:

$$
\left(1 + \frac{\Delta t}{\Delta x}\lambda_{i+\frac{1}{2}}^L - \frac{\Delta t}{\Delta x}\lambda_{i-\frac{1}{2}}^R\right) \geq 0.
$$

Hence, since $A_{i+\frac{1}{2}}^{L,*} > 0$ and $A_{i+\frac{1}{2}}^{R,*} > 0$, we obtain $A_i^{n+1} > 0 \; \forall i \in \mathbb{Z}$, because in (86) it is given by the sum of all positive quantities. The positivity of the intermediate states of the approximate Riemann solver is then a sufficient condition for A_i^{n+1} to be strictly positive.
Finally, we have to prove the well-balanced property *(3)* of the full numerical scheme. Let us assume that $(W_i^n)_{i\in\mathbb{Z}}$ defines a steady state. Hence, from Lemma 5 we have $W_{i+\frac{1}{2}}^{L,*} = W_i^n$ and $W_{i-\frac{1}{2}}^{R,*} = W_i^n$, which in turn yields $W_i^{n+1} = W_i^n$ for all $i \in \mathbb{Z}$. The proof of Lemma 6 is then achieved. □

We emphasize again that, from the above results, we obtain that the updated cross-sectional area A never vanishes and then the updated solution W_i^{n+1} always belongs to the physically admissible states space Ω, for all $i \in \mathbb{Z}$.
Furthermore, the same results and proofs obviously hold also for the approximate Riemann solver and the resulting numerical scheme extended to the generalized model with variable viscous resistance $R(x)$.

5. Second-order MUSCL extension of the fully well-balanced scheme

This section is devoted to a second-order extension of the fully well-balanced scheme derived in Section 3 based on a MUSCL procedure, involving a piecewise linear reconstruction of the approximate solution, in order to improve the space accuracy of the scheme. In addition, to be consistent in the order of accuracy, a second-order Runge-Kutta technique is adopted to increase also the time accuracy. Finally, the linear reconstruction is enriched by a procedure to recover the well-balanced property of the scheme.

5.1. The MUSCL reconstruction

We consider the MUSCL (Monotonic Upstream-Centred Scheme for Conservation Law) reconstruction technique, which belongs to a class of second-order methods (and,

in general, higher-order ones) suited to the framework of Godunov-type schemes, based on a reconstruction procedure (see [23, 15] for instance).
At time $t = t^n$ we know a piecewise constant approximate solution $(W_i^n)_{i\in\mathbb{Z}}$ of system (7). The MUSCL reconstruction procedure consists in replacing the constant state W_i^n in each cell I_i with a reconstruction polynomial vector $W_i^n(x)$ of a certain degree. This is done by finding a polynomial function for each component of the vector of conserved variables in each cell I_i. For the blood flow model (7), the variables to be reconstructed are A and q. Then, for the sake of simplicity, let us consider $w \in \{A, q\}$. In order to achieve a second-order space accuracy, we replace the constant state w_i^n with a linear approximation, that is a first-degree polynomial, in each cell $I_i = (x_{i-\frac{1}{2}}, x_{i+\frac{1}{2}})$, as follows:

$$w_i^n(x) = w_i^n + (x - x_i)\sigma_i^n, \tag{87}$$

where $\sigma_i^n := \sigma_i^n(w_{i-1}^n, w_i^n, w_{i+1}^n)$ is the limited slope of the linear reconstruction, to be defined. Then, the reconstructed variables at the inner interfaces of the cell I_i, the so-called boundary extrapolated values, are given by:

$$\begin{cases} w_i^- := w_i^n(x_{i-1/2}) = w_i^n\left(x_i - \dfrac{\Delta x}{2}\right) = w_i^n - \dfrac{\Delta x}{2}\sigma_i^n, \\ w_i^+ := w_i^n(x_{i+1/2}) = w_i^n\left(x_i + \dfrac{\Delta x}{2}\right) = w_i^n + \dfrac{\Delta x}{2}\sigma_i^n. \end{cases} \tag{88}$$

These values will be used in the numerical flux function $\mathcal{F}_{i+\frac{1}{2}}^n$ and in the numerical source term $\mathcal{S}_{i+\frac{1}{2}}^n$ of the Godunov-type scheme (64). We also note that $w_i^n(x_i) = w_i^n$, which means that the piecewise constant approximation is recovered at the centre of each cell. The MUSCL procedure is indeed an example of the so-called *conservative* reconstruction.
The last ingredient to be determined is the slope σ_i^n. We define σ_i^n as follows:

$$\sigma_i^n := \sigma_i^n(w_{i-1}^n, w_i^n, w_{i+1}^n) = \mathcal{L}\left(\frac{w_i^n - w_{i-1}^n}{\Delta x}, \frac{w_{i+1}^n - w_i^n}{\Delta x}\right) = \mathcal{L}\left(\Delta_{i-\frac{1}{2}}^n, \Delta_{i+\frac{1}{2}}^n\right), \tag{89}$$

where $\mathcal{L} : \mathbb{R} \times \mathbb{R} \to \mathbb{R}$ is a function whose arguments are the slopes between the constant states on each side of both interfaces of each cell I_i. Therefore, in order to define the MUSCL reconstruction, we need to provide an expression of $\mathcal{L}$ as a function of the two slopes $\Delta_{i-\frac{1}{2}}^n$ and $\Delta_{i+\frac{1}{2}}^n$. A natural, but rather useless choice for $\mathcal{L}$ may be the average between $\Delta_{i-\frac{1}{2}}^n$ and $\Delta_{i+\frac{1}{2}}^n$, but it is well-known that such a choice produces spurious oscillations, especially when the solution contains shocks. The use of a slope limiter is then strongly needed, in order to nullify or, at least, reduce the amplitude of these oscillations and to improve the stability of the scheme. There exists a very wide range of limiters among which the slope limiter can be selected. In this work, we have chosen the classical minmod slope limiter, given by:

$$\sigma_i^n = \operatorname{minmod}\left(\Delta_{i-\frac{1}{2}}^n, \Delta_{i+\frac{1}{2}}^n\right) = \operatorname{minmod}\left(\frac{w_i^n - w_{i-1}^n}{\Delta x}, \frac{w_{i+1}^n - w_i^n}{\Delta x}\right), \tag{90}$$

where the minmod function is defined as follows:

$$\operatorname{minmod}(x, y) = \begin{cases} x & \text{if } |x| \le |y| \text{ and } xy > 0, \\ y & \text{if } |x| > |y| \text{ and } xy > 0, \\ 0 & \text{if } xy \le 0. \end{cases} \tag{91}$$

Then, the resulting MUSCL scheme reads:

$$\begin{aligned} W_i^{n+1} = W_i^n - \frac{\Delta t}{\Delta x}\left[\mathcal{F}(W_i^+, W_{i+1}^-) - \mathcal{F}(W_{i-1}^+, W_i^-)\right] + \\ + \frac{\Delta t}{2}\left[\mathcal{S}(W_{i-1}^+, W_i^-) + \mathcal{S}(W_i^+, W_{i+1}^-)\right], \end{aligned} \tag{92}$$

where the numerical flux function $\mathcal{F}$ and the numerical source term $\mathcal{S}$ are defined as in (65) and (66), respectively, and the vectors W_i^- and W_i^+ contain all the components of the reconstructed variables at the inner interfaces of the cell I_i.
Now, the first issue we have to deal with concerns the robustness property of the MUSCL scheme (92). Indeed, in Section 4 we have proved that the first-order scheme derived in Section 3 preserves the positivity of the cross-sectional area A and, as a consequence, the same property has to be proved also for the second-order extension in space. This essential property involves only the variable A, which must be always strictly positive. Then, the following condition has to be satisfied:

$$\text{if } \forall i \in \mathbb{Z}: \quad A_i^n > 0 \quad \Longrightarrow \quad A_i^{n+1} > 0 \quad \forall i \in \mathbb{Z}.$$

In (7), the governing equation for the cross-sectional area A is homogeneous and does not contain any source terms. This means that the positivity of A does not depend on the friction source term S and its numerical approximation $\overline{S}$ within the scheme. In particular, this allows us to rewrite the MUSCL scheme (92) for A as a convex linear combination of first-order schemes, defined on the two sub-cells $(x_{i-\frac{1}{2}}, x_i)$ and $(x_i, x_{i+\frac{1}{2}})$ of each cell I_i. The two first-order schemes read:

$$\begin{cases} A_i^{n+1,-} = A_i^- - \dfrac{\Delta t}{\Delta x}\left[\mathcal{F}^A(A_i^-, A_i^+) - \mathcal{F}^A(A_{i-1}^+, A_i^-)\right], \\ A_i^{n+1,+} = A_i^+ - \dfrac{\Delta t}{\Delta x}\left[\mathcal{F}^A(A_i^+, A_{i+1}^-) - \mathcal{F}^A(A_i^-, A_i^+)\right]. \end{cases} \tag{93}$$

where the superscript A denotes the first component of the numerical flux function $\mathcal{F}$. We consider the following convex linear combination between $A_i^{n+1,-}$ and $A_i^{n+1,+}$:

$$\frac{1}{2}\left(A_i^{n+1,-} + A_i^{n+1,+}\right) = \frac{1}{2}\left(A_i^- + A_i^+\right) - \frac{\Delta t}{\Delta x}\left[\mathcal{F}^A(A_i^+, A_{i+1}^-) - \mathcal{F}^A(A_{i-1}^+, A_i^-)\right], \tag{94}$$

and, if we assume $\left(A_i^- + A_i^+\right)/2 = A_i^n$, then we exactly recover the MUSCL second-order scheme (92) for A, namely:

$$\frac{1}{2}\left(A_i^{n+1,-} + A_i^{n+1,+}\right) = A_i^n - \frac{\Delta t}{\Delta x}\left[\mathcal{F}^A(A_i^+, A_{i+1}^-) - \mathcal{F}^A(A_{i-1}^+, A_i^-)\right] = A_i^{n+1}. \tag{95}$$

As a consequence, thanks to the convexity, the MUSCL scheme conserves the same robustness property satisfied by the first-order scheme, ensuring the positivity preservation of the cross-sectional area A.

5.2. The Runge-Kutta-type method

By linear polynomial reconstruction, the derived scheme is second-order accurate in space, but it is only first-order accurate in time. Therefore, it is globally first-order accurate. In order to achieve the global second-order accuracy, we propose an extension of scheme (92) by using a Runge-Kutta-type method to provide a second-order time

accuracy.
We write the numerical scheme (64) under the condensed form:

$$\frac{W_i^{n+1} - W_i^n}{\Delta t} = \mathcal{H}(W^n). \tag{96}$$

Then, we adopt a second-order Runge-Kutta-type method, which consists in the following three steps:

- Evolution of $(W_i^n)_{i\in\mathbb{Z}}$ by a time Δt:

$$W_i^{n+1,-} = W_i^n + \Delta t\, \mathcal{H}(W^n); \tag{S1}$$

- Evolution of $\left(W_i^{n+1,-}\right)_{i\in\mathbb{Z}}$ by a time Δt:

$$W_i^{n+1,--} = W_i^{n+1,-} + \Delta t\, \mathcal{H}(W^{n+1,-}); \tag{S2}$$

- Convex linear combination between W_i^n and $W_i^{n+1,--}$ to compute the updated state W_i^{n+1}:

$$W_i^{n+1} = \frac{1}{2}\left(W_i^n + W_i^{n+1,--}\right). \tag{S3}$$

Since $A_i^n > 0$ and $A_i^{n+1,--} > 0$ for all $i \in \mathbb{Z}$, thanks to the convex combination step (S3), also in this case the robustness property is naturally satisfied by the resulting scheme and the positiveness of A is preserved, i.e. $A_i^{n+1} > 0$ for all $i \in \mathbb{Z}$.
Finally, by coupling the second-order MUSCL procedure in space with the second-order Runge-Kutta-type method in time, we obtain the sought globally second-order accurate numerical scheme.

5.3. Recovery of the well-balanced property

The second-order scheme proposed so far is not well-balanced. Indeed, the MUSCL reconstruction procedure modifies the approximate solution at the interfaces and, if W_i^n and W_{i+1}^n define a steady state, then the reconstruction step (88) provides reconstructed values W_i^+ and W_{i+1}^- that no longer define a steady state. Therefore, the scheme is second-order accurate in space and in time, but it is not able to exactly preserve the steady states. In order to restore this essential property, we propose the following strategy, which uses a steady state detector to detect whether two approximate solutions W_i^n and W_{i+1}^n, on the cells I_i and I_{i+1} respectively, define a steady state. To measure the deviation with respect to the equilibrium, the following quantity is defined at the interface $x_{i+\frac{1}{2}}$ between the cells I_i and I_{i+1}:

$$\|\mathrm{eq}_{i+\frac{1}{2}}^n\|_2 = \|\mathrm{eq}(W_i^n, W_{i+1}^n)\|_2 := \sqrt{|\mathcal{B}(W_{i+1}^n) - \mathcal{B}(W_i^n) + R\,\overline{q}_{i+\frac{1}{2}}^n \Delta x|^2 + |q_{i+1}^n - q_i^n|^2}, \tag{97}$$

where we have set:

$$\mathcal{B}(W_i^n) = -(q_i^n)^2 \log A_i^n + \frac{3}{5}\gamma (A_i^n)^{5/2} \quad \text{and} \quad \overline{q}_{i+\frac{1}{2}}^n = \overline{q}_{LR}(q_i^n, q_{i+1}^n) = \frac{q_i^n + q_{i+1}^n}{2}.$$

We immediately see that, if W_i^n and W_{i+1}^n define a steady state, then the quantity $\|\mathrm{eq}_{i+\frac{1}{2}}^n\|_2$ vanishes. Therefore, $\|\mathrm{eq}(W_L, W_R)\|_2$ detects whether a steady state is defined

by two states W_L and W_R.
In the same way, we can define the steady state detector between the three states W_{i-1}^n, W_i^n and W_{i+1}^n, i.e. for both pairs (W_{i-1}^n, W_i^n) and (W_i^n, W_{i+1}^n), as follows:

$$\|\mathrm{eq}_i^n\|_2 := \|\mathrm{eq}_{i-\frac{1}{2}}^n\|_2 + \|\mathrm{eq}_{i+\frac{1}{2}}^n\|_2, \tag{98}$$

which determines whether a steady state is present between the three states W_{i-1}^n, W_i^n and W_{i+1}^n, and, if that is the case, $\|\mathrm{eq}_i^n\|_2$ then vanishes.
At this point, we can use the steady state detector (98) to introduce a correction factor α in the reconstructed variables (88), which allows us to recover the well-balanced property of the scheme. We define:

$$\alpha := \frac{\|\mathrm{eq}_i^n\|_2}{\|\mathrm{eq}_i^n\|_2 + \Delta x^k}, \tag{99}$$

with $k \geq 2$, and thus we set:

$$w_i^{\pm} = w_i^n \pm \alpha \frac{\Delta x}{2} \sigma_i^n = w_i^n \pm \left(\frac{\|\mathrm{eq}_i^n\|_2}{\|\mathrm{eq}_i^n\|_2 + \Delta x^k} \right) \frac{\Delta x}{2} \sigma_i^n. \tag{100}$$

Point 2. The correcting factor α ensures that, when the states W_{i-1}^n, W_i^n and W_{i+1}^n are at equilibrium, the quantity $\|\mathrm{eq}_i^n\|_2$ detects the steady state, so that the first-order WB scheme is restored and the steady states are preserved. On the other hand, when we are far from equilibrium, we recover the usual MUSCL scheme with slope σ_i^n up to an error term of order Δx^{k+1}, which, for $k \geq 2$, is very small and does not significantly affect the slope and the reconstructed values $W_i^{\pm}$. Indeed, we have:

$$\alpha = \frac{\|\mathrm{eq}_i^n\|_2}{\|\mathrm{eq}_i^n\|_2 + \Delta x^k} \approxeq 1 + O(\Delta x^k),$$

so that

$$w_i^{\pm} = w_i^n \pm \alpha \frac{\Delta x}{2} \sigma_i^n \approxeq w_i^n \pm \frac{\Delta x}{2} \sigma_i^n + O(\Delta x^{k+1}). \tag{101}$$

This means that, for $k \geq 2$, we are adding a very small perturbation of order higher than 2. Hence, we are not perturbing the second-order accuracy of the scheme; the reconstruction is still second-order, as in the original MUSCL scheme.
The influence of the choice of the parameter k will be illustrated more in detail in Section 6 devoted to numerical experiments, to show that changing the value of k does not affect the numerical solution and the accuracy of the scheme. However, since the correcting factor α can be interpreted as a regularization of the Heaviside step function, it reasonable to avoid large values of k, otherwise α would be no longer continuous, and it would be equal either to 0 (at equilibrium) or 1 (elsewhere). As we will see in the numerical simulations, $k = 2$ usually works well. The idea is that the closer the states are to the equilibrium, the more the correcting factor will favour the first order WB scheme. End point 2.
By means of the above steady state detector, the resulting numerical scheme is thus globally second-order accurate, fully well-balanced and robust.

6. Numerical experiments

In this section, numerical experiments are carried out to test the derived scheme and to assess its properties, in particular the well-balanced property.

First, we test the fully well-balanced scheme derived for the model with constant viscous resistance $R > 0$, with source term discretization $\overline{S}$ given by (53), in both its first-order and second-order modes. Throughout the whole section, this numerical scheme is denoted by WB1. Afterwards, the fully well-balanced scheme extended to the model with variable viscous resistance $R(x)$, with source term discretization $\overline{S}$ given by (74), is adopted. This numerical scheme is denoted by WB2.
We present three sets of numerical experiments. The first set consists in the numerical validation of the proposed WB1 scheme. Since for the homogeneous blood flow system obtained by making the friction source term vanish in (7), i.e. by assuming $R = 0$, the exact solution to the Riemann problem is known, we test the WB1 scheme with several Riemann problems, by comparing the approximate solution with the exact Riemann solution. Afterwards, empirical convergence rates are computed for both the first-order and second-order WB1 schemes on a sequence of successively refined meshes by a factor of 3. Finally, the last set of numerical experiments assesses the well-balanced property of both the WB1 and WB2 schemes, by simulating the moving steady states exhibited in Section 2. Here, a simple counter-example of a numerical scheme which is not fully well-balanced is also proposed.
For all numerical tests, the geometrical parameters and mechanical properties of the vessel are summarized in Table 1. The other parameters and constants used within the numerical simulations are chosen according to Table 2. The choice of the boundary conditions is specified for each class of numerical experiments.

Parameter	**Name**	**Value**
r_0	Equilibrium radius	9.99×10^{-3} [m]
A_0	Equilibrium cross-sectional area	$\pi r_0^2 = 3.14 \times 10^{-4}$ [m^2]
h_0	Wall thickness	1.1×10^{-3} [m]
E	Young's modulus	4.0×10^5 [N/m^2]
ν	Poisson ratio	0.5
ρ	Blood density	1050 [Kg/m^3]
μ	Dynamic viscosity	0.0025 [Pa·s]
υ	Kinematic viscosity	μ/ρ
R	Viscous resistance	$22\pi\upsilon$

Table 1: Geometrical and mechanical parameters.

Parameter	**Name**	**Value**
M_{ex}	Number of cells for exact RP solutions	1000
M_{RP}	Number of cells for RPs	150
M_{WB}	Number of cells for WB experiments	200
CFL_1	Courant coefficient for first-order schemes	0.5
CFL_2	Courant coefficient for second-order schemes	0.25
ε_λ	Characteristic velocities cut-off in (39)	10^{-10} [m/s]
k	Steady state detector parameter in (100)	2

Table 2: Values of the computational parameters adopted in the numerical simulations.

6.1. *Validation experiments*

In order to verify that the WB1 scheme correctly approximates the solution of the blood flow equations (7), for this class of numerical tests we set $R = 0$ and we solve numerically the three Riemann problems shown in Table 3. We adopt the WB1 scheme in both its first-order and second-order modes and for each Riemann test we compare the numerical solution with the exact one.
We use $M_{RP} = 150$ computational cells for the numerical solution and $M_{ex} = 1000$ cells for the exact solution, over a spatial domain of length $L = 0.2$ m, with discontinuity located in $x_d = 0.1$ m. For this set of experiments, we impose homogeneous Neumann (transmissive) boundary conditions. The results are displayed in Figure 6.

Test Number	A_L	u_L	A_R	u_R	t_{end}	**Case**
(1)	$2A_0$	-1	$2A_0$	1	0.009 s	Two rarefactions
(2)	A_0	0	$2A_0$	0	0.012 s	Left shock + right rarefaction
(3)	$2A_0$	1	$2A_0$	-1	0.012 s	Two shocks

Table 3: Initial Conditions for the Riemann problems.

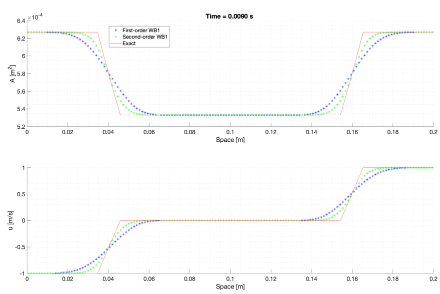

(a) RP(1)

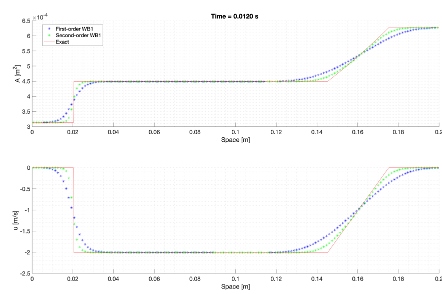

(b) RP(2)

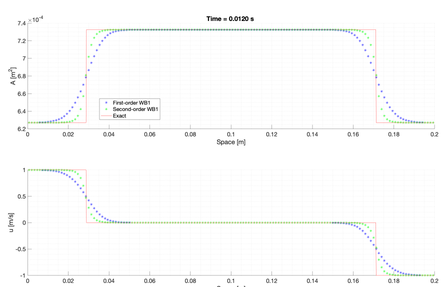

(c) RP(3)

Figure 6: Comparison between first-order WB1 scheme, second-order WB1 scheme and exact Riemann solver, for the cross-sectional area A and the blood velocity u along the vessel, testing the Riemann problems given in Table 3.

The results obtained with the fully well-balanced scheme are very satisfactory: the solutions to all Riemann problems are accurately approximated; there is good resolution of both smooth parts and discontinuities, the shocks are indeed correctly captured without spurious oscillations. In particular, this means also that the source term discretization $\overline{S}$ given by (53) is consistent with zero not only within rarefaction solutions, but also when discontinuous solutions are present. This behaviour suggests that with a mesh refinement the scheme converges to a solution which is very close to the exact one. Moreover, we can clearly see that the second-order accuracy of the scheme strongly improves the resolution of both rarefaction waves and shocks, significantly reducing the number of points within the discontinuity.

Point 2. In definition (99) of the correcting factor α, introduced in the reconstructed variables of MUSCL scheme to recover the well-balanced property, the parameter k has to be chosen such that $k \geq 2$ in order to ensure that the reconstruction is still second-order. However, as pointed out in Section 5, large values of k have to be avoided to preserve the continuity of the factor α. In all numerical experiments presented in this work, we have set $k = 2$. To show that the value $k = 2$ works well and to assess the influence of the choice of the parameter k on the numerical solution, we solve the RP(1) and RP(3) of Table 3 using the second-order WB1 scheme with several values of k. Figure 7 displays the results for $k = 2$, 2.5 and 3.
We clearly see that the numerical solutions obtained with the second-order WB1 scheme for different values of k (plotted in different colours: magenta, cyan and green) are almost indistinguishable, and we are only able to distinguish between exact solution, first-order and second-order numerical solutions. This means that, as expected, changing the value of k does not affect the numerical solution, since the very small perturbation introduced in the reconstructed values $W_i^{\pm}$ is of order higher than 2. End point 2.

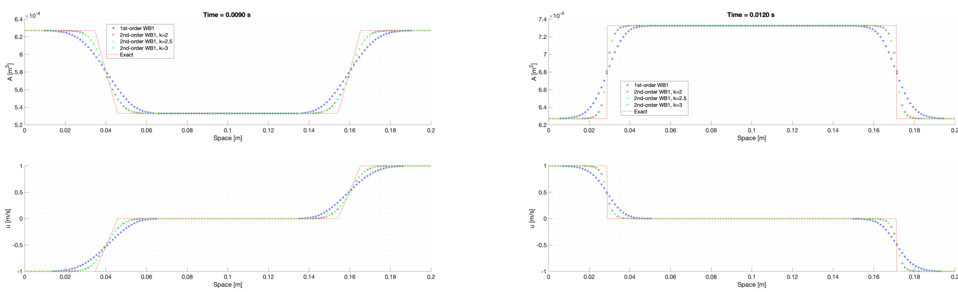

(a) RP(1) (b) RP(3)

Figure 7: Comparison between first-order WB1 scheme, second-order WB1 scheme for different values of k and exact Riemann solver, for the cross-sectional area A and the blood velocity u along the vessel, testing two of the Riemann problems given in Table 3.

6.2. Empirical convergence rates

Point 4. We turn now to verifying the order of accuracy of the second-order MUSCL scheme. To do that, we compute the empirical convergence rates for both the first-order and second-order WB1 schemes.
Since, except for the Riemann problem defined for the 1D model without source terms, we do not know an exact solution for the 1D blood flow equations, the order of accuracy

of the two schemes can not be estimated by computing the actual errors between the numerical solution and the exact one. However, these empirical convergence rates can be computed using the "errors" between two numerical solutions obtained with two successively refined computational meshes, by considering a smooth initial condition and a sufficiently small final time, in order to ensure that the numerical solution remains smooth in that time interval.
We emphasize once more that these "errors" are not the actual errors between the numerical and the exact solutions, but can be interpreted as the distance between successive numerical solutions obtained with progressively refined meshes and provide a practical way for estimating the order of accuracy of a scheme.
We consider the following sequence of successively refined meshes by a factor of 2:

$$M = \{40, 80, 160, 320, 640, 1280, 2560\}\,. \tag{102}$$

Then, we have:

$$M^{(j+1)} = 2M^{(j)} \quad \text{and} \quad \Delta x^{(j+1)} = \frac{\Delta x^{(j)}}{2},$$

where $\Delta x^{(j)}$ denotes the mesh size corresponding to mesh $M^{(j)}$. The vector containing the location of the centre of each cell and the numerical solution obtained with mesh $M^{(j)}$ are denoted, respectively, by:

$$x^{(j)} = \left(x_i^{(j)}\right)_{i=1,\dots,M^{(j)}} \qquad \text{and} \qquad \left(A^{(j)}, q^{(j)}\right) = \left\{\left(A_i^{(j)}, q_i^{(j)}\right)\right\}_{i=1,\dots,M^{(j)}}.$$

Given the computational meshes $M^{(j)}$ and $M^{(j+1)}$, the numerical solution corresponding to mesh $M^{(j)}$ is linearly interpolated at the finer points of $x^{(j+1)}$ obtained with mesh $M^{(j+1)}$, so that the "error" in any norm, namely L^1, L^2 or L^∞-norm, between the two numerical solutions $\left(A^{(j)}, q^{(j)}\right)$ and $\left(A^{(j+1)}, q^{(j+1)}\right)$, defined at identical points of $x^{(j+1)}$, can be computed as follows:

$$\begin{cases} \varepsilon^1_{j,j+1} = \Delta x^{(j+1)} \displaystyle\sum_{i=1}^{M^{(j+1)}} |A_i^{(j)} - A_i^{(j+1)}| + \Delta x^{(j+1)} \sum_{i=1}^{M^{(j+1)}} |q_i^{(j)} - q_i^{(j+1)}|, \\ \varepsilon^2_{j,j+1} = \sqrt{\Delta x^{(j+1)} \displaystyle\sum_{i=1}^{M^{(j+1)}} \left(A_i^{(j)} - A_i^{(j+1)}\right)^2 + \Delta x^{(j+1)} \sum_{i=1}^{M^{(j+1)}} \left(q_i^{(j)} - q_i^{(j+1)}\right)^2}, \\ \varepsilon^\infty_{j,j+1} = \displaystyle\max_{i=1,\dots,M^{j+1}} \left(|A_i^{(j)} - A_i^{(j+1)}| + |q_i^{(j)} - q_i^{(j+1)}|\right). \end{cases} \tag{103}$$

The order of accuracy p is then estimated as follows:

$$p = \frac{\log(\varepsilon_{j-1,j}) - \log(\varepsilon_{j,j+1})}{\log(2)}, \tag{104}$$

where ε is the error computed in any of the three norms introduced above.
By iterating this procedure on the sequence of successively refined meshes (102) for the WB1 scheme, we expect that the "errors" in all norms decrease as the mesh spacing Δx decreases and that the empirical convergence rates are achieved for both its first-order and second-order modes.
As smooth initial conditions, we consider a modified Riemann problem, which is the

smooth version of the two-rarefaction Riemann problem given in Table 3, defined by:

$$\begin{cases} A(x,0) = \begin{cases} A_L & \text{if } x \leq x_L, \\ \dfrac{A_L + A_R}{2} + \dfrac{A_L - A_R}{2} \cos\left(\pi \dfrac{2x_R - x_L}{x_R - x_L} - \pi \dfrac{x}{x_R - x_L}\right) & \text{if } x_L < x < x_R, \\ A_R & \text{if } x \geq x_R, \end{cases} \\ q(x,0) = \begin{cases} q_L & \text{if } x \leq x_L, \\ \dfrac{q_L + q_R}{2} + \dfrac{q_L - q_R}{2} \cos\left(\pi \dfrac{2x_R - x_L}{x_R - x_L} - \pi \dfrac{x}{x_R - x_L}\right) & \text{if } x_L < x < x_R, \\ q_R & \text{if } x \geq x_R, \end{cases} \end{cases} \tag{105}$$

with $L = 0.2$ m, $x_d = 0.1$, $x_L = x_d - 0.025$ and $x_R = x_d + 0.025$, $A_L = A_R = 2A_0$, $u_L = -1$ and $u_R = 1$, so that $q_L = A_L u_L$ and $q_R = A_R u_R$; and the following Gaussian wave:

$$\begin{cases} A(x,0) = A_0 + A_0\, \alpha\, e^{-\beta(x-x_d)^2}, \\ q(x,0) = 0, \end{cases} \tag{106}$$

with $L = 0.3$ m, $x_d = 0.15$, $\alpha = 1$ and $\beta = 1000$.
Moreover, in the first test case we take $t_{end} = 0.009$ s, while in the second one we set $t_{end} = 0.005$. Indeed, these final times are small enough to ensure that the numerical solution remains smooth.
The "errors" in L^1, L^2 and L^∞-norm between numerical solutions corresponding to progressively refined meshes, computed according to formulas (103), are summarized in Tables 4 and 5, for the modified Riemann problem IC and the Gaussian IC, respectively. The numerical solutions are obtained using the WB1 scheme in both its first-order and second-order modes.
This error analysis shows that, in all norms and for both numerical methods, the error decreases as the mesh spacing Δx decreases, or, equivalently, the number of computational cells M increases. Furthermore, we can observe that the errors obtained with the second-order scheme diminish faster than those corresponding to the first-order scheme. This means that, going on with the mesh refining, we expect that these errors will decrease at a convergence rate that depends on the order of accuracy of the specific numerical scheme adopted.

	First-order WB1 scheme			**Second-order WB1 scheme**		
M	L^1	L^2	L^∞	L^1	L^2	L^∞
40	-	-	-	-	-	-
80	2.6992e−06	6.1720e−06	2.5493e−05	1.7362e−06	4.4396e−06	2.0961e−05
160	1.4702e−06	3.5231e−06	1.6043e−05	5.8900e−07	1.6175e−06	0.9467e−05
320	7.5828e−07	1.9087e−06	0.9599e−05	1.6539e−07	5.3765e−07	4.1220e−06
640	3.8470e−07	1.0132e−06	5.5329e−06	4.5895e−08	1.7383e−07	1.7151e−06
1280	1.9351e−07	5.2850e−07	3.0783e−06	1.2409e−08	5.5382e−08	6.9499e−07
2560	0.9706e−07	2.7224e−07	1.6678e−06	3.3015e−09	1.7458e−08	2.7735e−07

Table 4: "Errors" in L^1, L^2 and L^∞-norm between successive numerical solutions obtained with the first-order and second-order WB1 scheme for the modified Riemann problem IC (105).

The empirical convergence rates, computed according to formula (104) on the sequence of refined meshes (102), are detailed in Tables 6 and 7 for the modified Riemann problem

	First-order WB1 scheme			Second-order WB1 scheme		
M	L^1	L^2	L^∞	L^1	L^2	L^∞
40	-	-	-	-	-	-
80	7.2819e−06	1.7816e−05	7.6324e−05	7.6383e−06	1.8474e−05	8.4161e−05
160	3.8236e−06	0.9426e−05	3.9741e−05	3.1867e−06	7.8658e−06	3.9032e−05
320	1.9570e−06	4.8375e−06	2.0087e−05	1.0982e−06	2.7792e−06	1.5212e−05
640	0.9913e−06	2.4504e−06	1.0101e−05	3.1178e−07	8.1103e−07	5.2268e−06
1280	4.9922e−07	1.2335e−06	5.0656e−06	8.8310e−08	2.3929e−07	2.0070e−06
2560	2.5054e−07	6.1890e−07	2.5366e−06	2.5030e−08	6.9909e−08	7.2449e−07

Table 5: "Errors" in L^1, L^2 and L^∞-norm between successive numerical solutions obtained with the first-order and second-order WB1 scheme for the Gaussian IC (106).

and the Gaussian ICs, respectively. From these tables, we conclude that, in any norm, the expected first-order and second-order convergence rates are demonstrated for the WB1 numerical scheme. This proves that the MUSCL-RK2 extension of the fully well-balanced scheme proposed is really second-order accurate in space and time. End point 4.

Scheme	Order of convergence p					
First-order WB1	$O(L^1)$	0.8766	0.9552	0.9790	0.9913	0.9954
	$O(L^2)$	0.8089	0.8843	0.9137	0.9389	0.9570
	$O(L^\infty)$	0.6681	0.7410	0.7948	0.8459	0.8841
Second-order WB1	$O(L^1)$	1.5596	1.8324	1.8495	1.8870	1.9102
	$O(L^2)$	1.4567	1.5890	1.6290	1.6514	1.6643
	$O(L^\infty)$	1.1467	1.1996	1.2651	1.3032	1.3253

Table 6: Empirical order of convergence p of the first-order and second-order WB1 scheme on the sequence of successively refined meshes (102) for the modified Riemann problem IC (105).

Scheme	Order of convergence p					
First-order WB1	$O(L^1)$	0.9294	0.9663	0.9812	0.9897	0.9946
	$O(L^2)$	0.9184	0.9627	0.9810	0.9902	0.9950
	$O(L^\infty)$	0.9415	0.9843	0.9918	0.9957	0.9979
Second-order WB1	$O(L^1)$	1.2612	1.5369	1.8166	1.8199	1.8189
	$O(L^2)$	1.2318	1.5009	1.7769	1.7610	1.7752
	$O(L^\infty)$	1.1085	1.3594	1.5412	1.3809	1.4700

Table 7: Empirical order of convergence p of the first-order and second-order WB1 scheme on the sequence of successively refined meshes (102) for the Gaussian IC (106).

6.3. Well-balanced assessment

In this second set of numerical experiments, we assess the well-balanced property of the derived scheme, i.e. the ability to exactly preserve and capture steady state solutions. In order to check the well-balancedness of the scheme, we consider moving steady states, characterized by a non-vanishing discharge q_0. Moreover, we fix the value of this uniform

discharge to $q_0 = -10^{-3}$ m^3/s.
In this subsection, we first present several numerical tests performed using the WB1 scheme; afterwards, numerical simulations adopting the WB2 scheme are carried out, to account for the presence of a variable viscous resistance $R(x)$ within the model.
Recall also that, when a moving steady state is imposed as initial condition, if we adopt a numerical scheme that is fully well-balanced, then we expect that this scheme exactly preserves in time the steady state initial condition. To assess this behaviour, the errors in L^1 and L^2 norms between the steady state initial condition $W_i^{SS} = (A_i^{SS}, q_i^{SS})$ and the numerical solution $W_i^n = (A_i^n, q_i^n)$ at a certain time t^n are computed according to the following formulas:

$$\begin{aligned} \varepsilon_1 &= \Delta x \sum_{i=1}^{M} |A_i^n - A_i^{SS}| + \Delta x \sum_{i=1}^{M} |q_i^n - q_i^{SS}|, \\ \varepsilon_2 &= \sqrt{\Delta x \sum_{i=1}^{M} (A_i^n - A_i^{SS})^2 + \Delta x \sum_{i=1}^{M} (q_i^n - q_i^{SS})^2}. \end{aligned} \tag{107}$$

Let now $R > 0$ be a constant parameter, whose value is given in Table 1. We impose as initial condition a steady state, computed in Section 2 and displayed in Figure 1. In particular, for the cross-sectional area we select the upper branch (dotted) of these steady state solutions. Dirichlet boundary conditions are prescribed.
Then, the numerical solution is evolved in time and the L^1 and L^2 errors between the steady state initial condition and the numerical solution at times $t_{end} = 0.1$ s, 1 s and 5 s are computed. These errors are presented in Table 8. From this errors analysis, we

	L^1-Errors			**L^2-Errors**		
Scheme	$t = 0.1$ s	$t = 1$ s	$t = 5$ s	$t = 0.1$ s	$t = 1$ s	$t = 5$ s
First-order WB1	1.11e−14	6.68e−15	3.57e−15	7.88e−15	5.96e−15	5.92e−15
Second-order WB1	1.07e−14	6.69e−15	3.68e−15	7.50e−15	5.95e−15	5.90e−15

Table 8: L^1-errors and L^2-errors between the steady state initial condition and the numerical solution computed at different times, for the moving steady state experiment with constant viscous resistance R and Dirichlet boundary conditions.

conclude that the moving steady state is exactly captured and preserved in time by the scheme. In particular, in the second-order scheme, the steady state detector given by (98) detects the steady state, the limited slopes of the MUSCL linear reconstruction vanish and the well-balanced property is then recovered.

A steady state solution represents a boundary value problem (BVP). Then, an important issue concerns the choice of the boundary conditions to be imposed at the boundaries of the vessel. In particular, if a scheme is fully well-balanced, then we expect that, by imposing arbitrary smooth initial conditions and the correct boundary conditions, after a sufficiently long time the steady state is restored by the scheme. Indeed, a long final time allows the perturbations or the oscillations present in the initial conditions to be dissipated and the original steady state to be recovered.

We impose the following smooth initial conditions:

$$\begin{cases} A(x,t=0) = A_0 + A_0\,\delta\,\sin\left(\dfrac{2\pi}{L}x\right), \\ q(x,t=0) = q_0 - q_0\,\delta\,\cos\left(\dfrac{2\pi}{L}x\right), \end{cases} \tag{108}$$

where $\delta = 0.1$ is a perturbation and L is the length of the space domain. The steady state reference solution and the smooth initial condition (108) are plotted together in Figure 8. We prescribe the following *mixed* boundary conditions: on the left boundary,

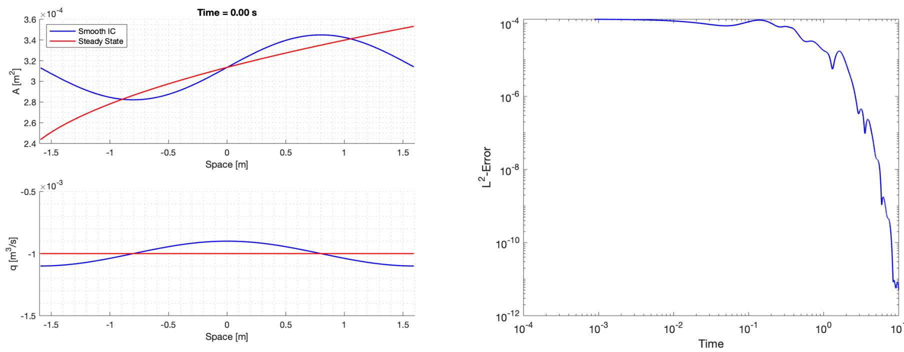

(a) (b)

Figure 8: (a) Steady state reference solution (red) and smooth initial condition (108) (blue) for the well-balanced property assessment, with constant viscous resistance R. (b) Evolution in time of the L^2-error in logarithmic scale between the numerical solution computed with the first-order WB1 scheme and the steady state reference solution.

we choose Dirichlet BC for A and non-homogeneous Neumann BC for q; conversely, on the right boundary, we prescribe non-homogeneous Neumann BC for A and Dirichlet BC for q. This choice corresponds to negative flow $q_0 < 0$ from the right inlet of the vessel, where an input flux is imposed, towards the left outlet.
By adopting again the WB1 scheme, we compute the L^1 and L^2 errors between the numerical solution and the steady state reference solution, at times $t = 1$ s, 5 s and 10 s. These errors are given in Table 9. The errors analysis shows that both the L^1 and L^2 errors sharply decrease in time and converge, indicating that, for a sufficiently large final time, the scheme recovers the original unperturbed steady state solution, as expected. Moreover, the temporal evolution of the L^2-error is depicted in Figure 8 for the first-order WB1 scheme. These results prove once again the well-balanced property of the scheme.
Point 3. We emphasize that the "errors" summarized in Table 9 are computed between the numerical solution obtained with the first-order and the second-order WB1 schemes at several time instants and the steady state reference solution, not the exact solution. To be precise, these "errors" should be rather referred to as convergence errors in time toward the steady state. Then, since these are not the actual errors between the numerical solution and the exact one, we do not expect to obtain a smaller error when adopting the second-order scheme. Indeed, as we can observe from Table 9, the errors for the first-order and second-order schemes are comparable, since the order of accuracy of the scheme does not affect the rate at which the numerical solution converges to the

steady state, but to the exact solution. End point 3.

	L^1-Errors			L^2-Errors		
Scheme	$t = 1$ s	$t = 5$ s	$t = 10$ s	$t = 1$ s	$t = 5$ s	$t = 10$ s
First-order WB1	3.50e−05	3.66e−08	9.75e−12	1.80e−05	2.02e−08	5.18e−12
Second-order WB1	3.53e−05	4.36e−08	9.92e−12	1.82e−05	2.37e−08	5.25e−12

Table 9: L^1-errors and L^2-errors between the steady state reference solution and the numerical solution computed at different times, with smooth initial condition (108), constant viscous resistance R and mixed boundary conditions.

To conclude this section, we turn now to assess the well-balancing of the WB2 scheme suited to the generalized blood flow model, including a variable viscous resistance $R(x)$ that is a prescribed function with respect to the space variable x. Recall that, in this case, the steady states are given by equations (19). In particular, for any suitable choice of the function $x \mapsto R(x)$, the approximate steady state solutions of system (7) must satisfy the following relations:

$$\begin{cases} q_i = q_0, \\ \mathcal{F}_{q_0}(A_i) - \mathcal{F}_{q_0}(A_{ref}) = \sum_{j=0}^{i-1} \Big(\mathcal{F}_{q_0}(A_{j+1}) - \mathcal{F}_{q_0}(A_j) \Big) = -q_0 \sum_{j=0}^{i-1} \mathcal{Q}(R, x_j, x_{j+1}), \end{cases} \tag{109}$$

for all $i \in \mathbb{Z}$, where the function $\mathcal{F}_{q_0}$ is given by (16) and $\mathcal{Q}$ denotes a suitable quadrature formula to approximate the integral of the function $R(x)$, as defined in (20).
Point 5. In this work, in all numerical experiments performed with variable viscous resistance $R(x)$, a six-point Gaussian-Legendre quadrature formula is used. End point 5.
In order to assess the well-balancedness of the WB2 scheme equipped with the source term discretization (74), we have to check that, if a moving steady state is imposed as initial condition, then this steady state is exactly preserved in time by the scheme.
We test the WB2 numerical scheme for different choices of the function $R(x)$. As preliminary test, we consider again the case of constant R, then we select the following functions:

$$\begin{aligned} R_1(x) &= \big(1 + \cos^2(x)\big) \cdot 10^{-4} > 0 && \text{for any } x \in \mathbb{R}, \\ R_2(x) &= \big(4 - x^2\big) \cdot 10^{-4} > 0 && \text{for } x \in (-2, 2), \\ R_3(x) &= R + R\,\delta_R \sin\left(\frac{2\pi}{L} x\right) > 0 && \text{for any } x \in \mathbb{R}. \end{aligned} \tag{110}$$

The function $R_3(x)$ attains values that oscillate around the reference constant value R, given in Table 1, with $\delta_R = 0.1$ being a perturbation and L the length of the space domain.
It is worth noting that no physical or biomedical considerations have been made to model the function $R(x)$, but the above functions have been chosen in a way to ensure that $R(x)$ is positive on the whole computational domain and attains values within the correct physical range of this parameter.
For each choice of the function $R(x)$ in (110), a steady state solution is computed and imposed as initial condition. For instance, the approximate steady state obtained for $R = R_3(x)$, with $L = 1.5$ m, is displayed in Figure 9.

Then, the numerical solution is evolved in time by adopting the WB2 scheme and we compute the L^1 and L^2 errors between the numerical solution and the steady state initial condition, at times $t_{end} = 0.1$ s, 1 s and 5 s. These errors are exhibited in Table 10. As usual for the well-balanced assessment experiments, we prescribe Dirichlet boundary conditions.
As expected, in all cases the moving steady state is exactly preserved by the scheme, which proves that the WB2 scheme is fully well-balanced.

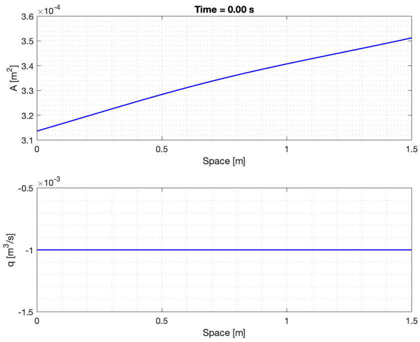

Figure 9: Steady state initial condition for variable viscous resistance $R = R_3(x)$.

	L^1-Errors			L^2-Errors		
Viscous resistance	$t = 0.1$ s	$t = 1$ s	$t = 5$ s	$t = 0.1$ s	$t = 1$ s	$t = 5$ s
$R = 22\pi\mu/\rho$	5.70e−15	1.31e−15	1.29e−15	6.89e−15	3.29e−15	3.29e−15
$R_1(x)$	5.24e−15	1.21e−15	1.19e−15	6.60e−15	3.26e−15	3.27e−15
$R_2(x)$	2.48e−15	6.25e−16	6.07e−16	3.63e−15	2.31e−15	2.31e−15
$R_3(x)$	5.30e−15	1.22e−15	1.20e−15	6.53e−15	3.19e−15	3.19e−15

Table 10: L^1-errors and L^2-errors between the steady state initial condition and the numerical solution computed at different times, for different choices of the function $R(x)$.

We consider now the last type of numerical experiments, through which we want also to compare the performance of the fully well-balanced scheme WB2 with respect to a standard non-well-balanced numerical scheme. Indeed, in order to emphasize once again the necessity of the new approach proposed in this work to construct a fully well-balanced scheme for the 1D blood flow model and the crucial role played by the source term discretization in such a scheme, we now provide a simple counter-example of a finite volume scheme in which the steady state solutions are not preserved. For this purpose, we adopt the HLL numerical flux coupled with a centred approximation of the source term.
We consider smooth initial conditions for A and q, as follows:

$$\begin{cases} A(x, t = 0) = A_0(x), \\ q(x, t = 0) = q_0, \end{cases} \tag{111}$$

which prescribe a uniform discharge q_0. If, enforcing $\partial_t q = 0$, we define the variable viscous resistance $R(x)$ at steady state as follows:

$$R(x) = -\frac{A_0(x)}{q_0}\partial_x\left(\frac{q_0^2}{A_0(x)} + \gamma(A_0(x))^{3/2}\right), \tag{112}$$

then the exact solution of system (7) will be:

$$\begin{cases} A(x,t) = A_0(x), \\ q(x,t) = q_0, \end{cases} \tag{113}$$

for any $t \in \mathbb{R}^+$.
Therefore, if the numerical scheme is not well-balanced, the steady state will be completely lost by the scheme. On the other hand, if the numerical scheme is fully well-balanced, we expect the initial condition (111) to be a steady state solution of the blood flow system (7) and to be exactly preserved in time by the scheme, as soon as the viscous resistance R is defined at equilibrium, according to formula (112).
In particular, expression (112) of $R(x)$ can be rewritten as follows:

$$\begin{aligned} R(x) &= -\frac{A_0(x)}{q_0}\left(-\frac{q_0^2}{(A_0(x))^2}\partial_x A_0(x) + \frac{3}{2}\gamma(A_0(x))^{1/2}\partial_x A_0(x)\right) = \\ &= \left(\frac{q_0}{A_0(x)} - \frac{3}{2}\gamma\frac{(A_0(x))^{3/2}}{q_0}\right)A_0'(x). \end{aligned} \tag{114}$$

Then, for any choice of the smooth, strictly positive function $A_0(x)$, a primitive of the function $R(x)$ given by (114) read:

$$\Phi_R(x) = \int R(x)\,dx = q_0\log(A_0(x)) - \frac{3}{5}\gamma\frac{(A_0(x))^{5/2}}{q_0} + c, \tag{115}$$

with $c \in \mathbb{R}$, and integration of the function $R(x)$ within the definition (74) of the source term discretization $\overline{S}$ becomes exact, namely

$$\begin{aligned} \mathcal{Q}(R, x_L, x_R) &= \int_{x_L}^{x_R} R(x)\,dx = \Phi_R(x_R) - \Phi_R(x_L) = \\ &= q_0\log(A_0(x_R)) - \frac{3}{5}\gamma\frac{(A_0(x_R))^{5/2}}{q_0} - q_0\log(A_0(x_L)) + \frac{3}{5}\gamma\frac{(A_0(x_L))^{5/2}}{q_0}. \end{aligned} \tag{116}$$

As a consequence, the steady state initial condition must be exactly preserved by the fully well-balanced scheme.
We consider the following two pairs of smooth initial conditions:

$$\begin{cases} A(x,t=0) = A_0^{(1)}(x) = A_0 + A_0\,\delta_A\,\sin\left(\frac{2\pi}{L}x\right), \\ q(x,t=0) = q_0, \end{cases} \tag{117}$$

$$\begin{cases} A(x,t=0) = A_0^{(2)}(x) = A_0 + A_0\,\delta_A\left[\cos\left(\frac{2\pi}{L}x\right)\right]^2, \\ q(x,t=0) = q_0, \end{cases} \tag{118}$$

where $\delta_A = 0.1$ is a perturbation and L is the length of the space domain.
We first consider the initial condition (117) and the numerical scheme with HLL numerical

flux and centred approximation of the source term, which is not fully well-balanced. Dirichlet boundary conditions are prescribed.
As expected, the steady state is captured with a very large error and, just after the first time steps, the numerical solution moves away from the initial condition. We conclude that the steady state is not preserved by this scheme, as we clearly see from Figure 10, where the initial condition (117) and the numerical solution computed at time $t = 0.01$ s are displayed.

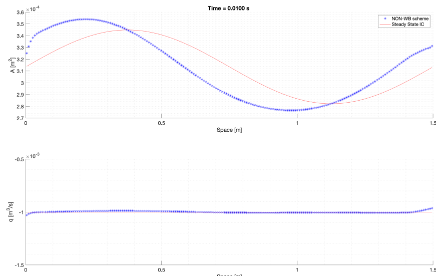

Figure 10: Steady state initial condition (117) and numerical solution at time $t_{end} = 0.01$ s evolved by adopting the non-fully-well-balanced scheme with variable viscous resistance $R(x)$ defined by (114).

Conversely, by using the WB2 scheme and definition (114) for the viscous resistance $R(x)$ at equilibrium, thanks to the well-balancing of the scheme, when we impose both initial conditions (117) and (118), we obtain that the numerical solution does not move in time and the steady state initial conditions are exactly preserved by the scheme. Dirichlet boundary conditions are prescribed.
The L^1 and L^2 errors between the numerical solution computed at time $t_{end} = 1$ s and the steady state initial conditions (117) and (118) are presented in Table 11. These results prove once again that the derived scheme is fully well-balanced.

IC	**L^1-Errors**	**L^2-Errors**
$(A_0^{(1)}, q_0)$	3.23e−18	2.31e−18
$(A_0^{(2)}, q_0)$	4.21e−18	3.27e−18

Table 11: L^1-errors and L^2-errors between each set of steady state initial conditions (117) and (118) and the numerical solution computed at time $t_{end} = 1$ s by adopting the WB2 numerical scheme.

7. Concluding remarks and future work

In this work, we first have studied the moving steady state solutions of the one-dimensional blood flow equations with friction source term. Afterwards, a Godunov-type scheme for this system has been constructed, which is fully well-balanced and preserves the positivity of the cross-sectional area. Then, we have proposed a modification of this scheme, suited for the generalized model including a space-variable viscous resistance. A second-order well-balanced MUSCL extension of the scheme has also been derived.

Finally, several numerical experiments have been performed to validate the numerical scheme and assess its properties, in particular the well-balanced property.

Future work will include the extension of the proposed well-balanced strategy to take into account and discretize other types of source terms, which arise when a more realistic 1D blood flow model is considered, with varying geometrical and mechanical properties of the vessel. In fact, in the modelling of many physiological and pathological situations of interest, such as the placement of a stent, the presence of a stenosis or simply the occurrence of physiological variations, it is relevant to consider the variation, even discontinuous, of geometrical and mechanical properties of the vessel, which generate additional geometric-type source terms. Then, in the fashion of the well-balanced strategy designed so far, suitable discretizations of these new source terms need to be introduced in order to preserve the well-balanced and robustness properties of the scheme.

References

[1] J. Alastruey, A. W. Khir, K. S. Matthys, P. Segers, S. J. Sherwin, P. R. Verdonck, K. H. Parker, and J. Peiró. Pulse wave propagation in a model human arterial network: Assessment of 1-D visco-elastic simulations against in vitro measurements. *Journal of Biomechanics*, 44:2250–2258, 2011.

[2] E. Audusse, F. Bouchut, M. O. Bristeau, R. Klein, and B. Perthame. A fast and stable well-balanced scheme with hydrostatic reconstruction for shallow water flows. *SIAM J. Scientific Computing*, 25(6):2050–2065, 2004.

[3] A. Bermudez and M. E. Vazquez. Upwind methods for hyperbolic conservation laws with source terms. *Computers & Fluids*, 23(8):1049 – 1071, 1994.

[4] C. Berthon and C Chalons. A fully well-balanced, positive and entropy-satisfying Godunov-type method for the shallow-water equations. *Mathematics of Computation*, 85(299):1281–1307, 2016.

[5] C. Berthon, C. Chalons, S. Cornet, and G. Sperone. Fully well-balanced, positive and simple approximate Riemann solver for shallow water equations. *Bulletin of the Brazilian Mathematical Society (N.S.)*, 47(1):117–130, 2016.

[6] P. J. Blanco, S. M. Watanabe, M. A. Passos, P. A. Lemos, and R. A. Feijóo. An anatomically detailed arterial network model for one-dimensional computational hemodynamics. *IEEE Transactions on Biomedical Engineering*, 62(2):736–753, 2014.

[7] M. J. Castro, A. Pardo Milanés, and C. Parés. Well-balanced numerical schemes based on a generalized hydrostatic reconstruction technique. *Mathematical Models and Methods in Applied Sciences*, 17(12):2055–2113, 2007.

[8] O. Delestre and P. Y. Lagrée. A "well-balanced" finite volume scheme for blood flow simulation. *International Journal for Numerical Methods in Fluids*, 72(2):177–205, 2013.

[9] L. Formaggia, D. Lamponi, and A. Quarteroni. One-dimensional models for blood flow in arteries. *Journal of Engineering Mathematics*, 47:251–276, 2003.

[10] L. Formaggia, A. Quarteroni, and A. Veneziani. *Cardiovascular Mathematics: Modeling and Simulation of the Circulatory System.* Modeling, Simulation and Applications. Springer, 2009.

[11] S. K. Godunov. A finite difference method for the numerical computation of discontinuous solutions of the equations of fluid dynamics. *Mat. Sb.*, 47:357–393, 1959.

[12] L. Gosse. A well-balanced flux-vector splitting scheme designed for hyperbolic systems of conservation laws with source terms. *Computers & Mathematics with Applications*, 39(9):135 – 159, 2000.

[13] J. M. Greenberg and A. Y. LeRoux. A well-balanced scheme for the numerical processing of source terms in hyperbolic equations. *SIAM Journal on Numerical Analysis*, 33(1):1–16, 1996.

[14] A. Harten, D. P. Lax, and B. van Leer. On upstream differencing and Godunov-type schemes for hyperbolic conservation laws. *SIAM Rev*, 25(1):35–61, 1983.

[15] R. J. LeVeque. *Finite Volume Methods for Hyperbolic Problems.* Cambridge Texts in Applied Mathematics. Cambridge University Press, Cambridge, 2002.

[16] V. Michel-Dansac, C. Berthon, S. Clain, and F. Foucher. A well-balanced scheme for the shallow-water equations with topography. *Comput. Math. Appl.*, 72(3):568–593, 2016.

[17] V. Michel-Dansac, C. Berthon, S. Clain, and F. Foucher. A well-balanced scheme for the shallow-water equations with topography or Manning friction. *Journal of Computational Physics*, 335:115 – 154, 2017.

[18] L. O. Müller, C. Parés, and E. F. Toro. Well-balanced high-order numerical schemes for one-dimensional blood flow in vessels with varying mechanical properties. *Journal of Computational Physics*, 242:53–85, 2013.

[19] L. O. Müller and E. F. Toro. Well-balanced high-order solver for blood flow in networks of vessels with variable properties. *International Journal for Numerical Methods in Biomedical Engineering*, 29:1388–1411, 2013.

[20] L. O. Müller and E. F. Toro. A global multiscale mathematical model for the human circulation with emphasis on the venous system. *International Journal for Numerical Methods in Biomedical Engineering*, 30:681–725, 2014.

[21] C. Parés. Numerical methods for nonconservative hyperbolic systems: A theoretical framework. *SIAM Journal on Numerical Analysis*, 44:300–321, 2006.

[22] S. J. Sherwin, L. Formaggia, J. Peiró, and V. Franke. Computational modeling of 1D blood flow with variable mechanical properties and application to the simulation of wave propagation in the human arterial system. *Int. J. Numer. Meth. Fluids*, 43:673–700, 2003.

[23] E. F. Toro. *Riemann Solvers and Numerical Methods for Fluid Dynamics: A Practical Introduction.* Springer-Verlag Berlin Heidelberg, 2009. Third Edition.

[24] E. F. Toro. Brain venous haemodynamics, neurological diseases and mathematical modelling. A review. *Applied Mathematics and Computation*, 272:542 – 579, 2016. Recent Advances in Numerical Methods for Hyperbolic Partial Differential Equations.

[25] E. F. Toro and A. Siviglia. *Simplified blood flow model with discontinuous vessel properties: Analysis and exact solutions.* Modelling Physiological Flows Series: Modelling, Simulation and Applications. D. Ambrosi, A. Quarteroni and G. Rozza (Eds.). Springer-Verlag, 2012.

[26] E. F. Toro and A. Siviglia. Flow in collapsible tubes with discontinuous mechanical properties: Mathematical model and exact solutions. *Communications in Computational Physics*, 13(2):361–385, 2013.